

University of Groningen

Size scaling of photophysiology and growth in four freshly isolated diatom species from Ryder Bay, western Antarctic peninsula

Kulk, Gemma; Buist, Anton; van de Poll, Willem H; Rozema, Patrick D; Buma, Anita G J

Published in:
Journal of Phycology

DOI:
[10.1111/jpy.12813](https://doi.org/10.1111/jpy.12813)

IMPORTANT NOTE: You are advised to consult the publisher's version (publisher's PDF) if you wish to cite from it. Please check the document version below.

Document Version
Publisher's PDF, also known as Version of record

Publication date:
2019

[Link to publication in University of Groningen/UMCG research database](#)

Citation for published version (APA):

Kulk, G., Buist, A., van de Poll, W. H., Rozema, P. D., & Buma, A. G. J. (2019). Size scaling of photophysiology and growth in four freshly isolated diatom species from Ryder Bay, western Antarctic peninsula. *Journal of Phycology*, 55(2), 314-328. <https://doi.org/10.1111/jpy.12813>

Copyright

Other than for strictly personal use, it is not permitted to download or to forward/distribute the text or part of it without the consent of the author(s) and/or copyright holder(s), unless the work is under an open content license (like Creative Commons).

The publication may also be distributed here under the terms of Article 25fa of the Dutch Copyright Act, indicated by the "Taverne" license. More information can be found on the University of Groningen website: <https://www.rug.nl/library/open-access/self-archiving-pure/taverne-amendment>.

Take-down policy

If you believe that this document breaches copyright please contact us providing details, and we will remove access to the work immediately and investigate your claim.

Downloaded from the University of Groningen/UMCG research database (Pure): <http://www.rug.nl/research/portal>. For technical reasons the number of authors shown on this cover page is limited to 10 maximum.

SIZE SCALING OF PHOTOPHYSIOLOGY AND GROWTH IN FOUR FRESHLY ISOLATED DIATOM SPECIES FROM RYDER BAY, WESTERN ANTARCTIC PENINSULA¹

Gemma Kulk,²  Anton Buist, Willem H. van de Poll, Patrick D. Rozema

Department of Ocean Ecosystems, Energy and Sustainability Research Institute Groningen, University of Groningen, Nijenborgh 7, 9747 AG, Groningen, the Netherlands

and Anita G. J. Buma

Department of Ocean Ecosystems, Energy and Sustainability Research Institute Groningen, University of Groningen, Nijenborgh 7, 9747 AG, Groningen, the Netherlands

Arctic Centre, Faculty of Arts, University of Groningen, Aweg 30, 9718 CW, Groningen, the Netherlands

Diatoms are one of the dominant groups in phytoplankton communities of the western Antarctic Peninsula (WAP). Although generally well-studied, little is known about size dependent photophysiological responses in diatom bloom formation and succession. To increase this understanding, four Antarctic diatom species covering two orders of magnitude in cell size were isolated in northern Marguerite Bay (WAP). *Fragilariopsis* sp., *Pseudo-nitzschia* cf. *subcurvata*, *Thalassiosira* cf. *antarctica*, and *Proboscia* cf. *alata* were acclimated to three different irradiances after which photophysiology, electron transport, carbon fixation, and growth were assessed. The small species *Fragilariopsis* sp., *Pseudo-nitzschia* cf. *subcurvata*, and large species *Proboscia* cf. *alata* showed similar photoacclimation to higher irradiances with a decrease in cellular chlorophyll *a* and an increase in chlorophyll *a* specific absorption and xanthophyll cycle pigments and activity. In contrast, pigment concentrations and absorption remained unaffected by higher irradiances in the large species *Thalassiosira* cf. *antarctica*. Overall, the small species showed significantly higher growth rates compared to the large species, which was related to relatively high light harvesting capacity and electron transport rates in the smaller species. However, photophysiological responses related to photoinhibition and photoprotection and carbon fixation showed no relationship with cell size. This study supports the dominance of small diatoms at low irradiances during winter and early spring, but does not provide photophysiological evidence for the dominance of large diatoms during the phytoplankton bloom in the WAP. This suggests that other factors such as grazing and nutrient availability are likely to play a major role in diatom bloom formation.

Key index words: carbon uptake; diatoms; electron transport; photophysiology; size scaling; west Antarctic peninsula

Abbreviations: ¹⁴C, carbon-14; \bar{a}^* , spectrally weighted mean specific absorption coefficient; C: Chl *a*, carbon to chlorophyll *a* ratio; Dd, diadinoxanthin; DPS, de-epoxidation state of the xanthophyll pigment cycle; Dt, diatoxanthin; ETR, electron transport rate; ETR_{max}, maximum electron transport rate; Ek_{ETR}, photoacclimation index of electron transport; Ek, photoacclimation index of carbon fixation; F₀, minimum fluorescence in the dark-adapted state; F_m['], maximum fluorescence in the light; F_m^o, maximum fluorescence in the dark-adapted state; F_m^r, maximum fluorescence in the absence of fast relaxing non-photochemical quenching; F_v, steady-state fluorescence; Fuco, fucoxanthin; F_v/F_m, maximum quantum yield of photosystem II; NPQ_F, fast non-photochemical quenching; NPQ, non-photochemical quenching; NPQ_S, slowly non-photochemical quenching; PAM, pulse amplitude modulation; PE, photosynthesis versus irradiance; P_{max}, maximum carbon fixation rate; POC, particulate organic carbon; RaTS, rothera oceanographic and biological time series; S/V, surface-to-volume ratio; SSE, size scaling exponents; WAP, western Antarctic peninsula; α_{ETR} , initial slope of electron transport; α , initial slope of carbon fixation; β -car, β -carotene; μ , growth rate; $\Phi_{e,C}$, electron requirement of carbon fixation; Φ_{PSII} , quantum yield of photosystem II

Diatoms are one of the dominant taxonomic groups in coastal phytoplankton communities of the western Antarctic peninsula (WAP; Garibotti et al. 2003, Piquet et al. 2011, Rozema et al. 2017). The depth and geographic distribution of Antarctic diatoms and other taxonomic groups can be explained by their response to water column conditions (Garibotti et al. 2003, Piquet et al. 2011, Rozema et al.

¹Received 31 August 2017. Accepted 19 October 2018. First Published Online 18 November 2018. Published Online 29 January 2019, Wiley Online Library (wileyonlinelibrary.com).

²Author for correspondence: e-mail g.kulk@rug.nl.

Editorial Responsibility: K. Valentin (Associate Editor)

2017). For example, diatoms thrive under shallow mixed water column conditions with relatively high, stable irradiance conditions, whereas haptophytes such as *Phaeocystis* spp. thrive under more deeply mixed conditions where short periods of darkness are interchanged with periods of excess irradiance at the surface (Arrigo et al. 1999, Kropuenske et al. 2009, Mills et al. 2010, Rozema et al. 2017). In the well-studied northern Marguerite Bay, water column stability and the consequent irradiance climate phytoplankton experience are believed to control the onset of the phytoplankton bloom in spring (Clarke et al. 2008, Venables et al. 2013). The water column conditions in spring and summer are influenced by the preceding winter conditions, with the extent and duration of sea ice cover determining the strength of summer stratification and consequent mixed layer depth (Venables et al. 2013). Years with reduced sea ice cover are characterized by a deeply mixed water column in winter followed by a weaker stratified water column in summer and low biomass during the phytoplankton growth season (Meredith et al. 2010, Venables et al. 2013). Because diatoms play an important role in the Antarctic food web and carbon sequestering to the ocean's interior (Anadón and Estrada 2002, Ducklow et al. 2007), it is essential to understand how Antarctic diatoms respond to changes in water column conditions and how this influences the succession of the phytoplankton bloom.

Phytoplankton bloom dynamics in northern Marguerite Bay are well-studied due to the presence of the Rothera Oceanographic and Biological Time Series (RaTS) station, located in Ryder Bay just off Adelaide Island (Clarke et al. 2008, Venables et al. 2013, Rozema et al. 2017). Although interannual variations exist, the phytoplankton bloom in Ryder Bay typically peaks in December and January with chlorophyll *a* concentrations reaching up to 20–25 mg · m⁻³ and is often followed by a second bloom in March (Clarke et al. 2008, Venables et al. 2013). The phytoplankton peak is dominated by larger microphytoplankton (>20 µm), whereas smaller pico- (<2 µm) and nanophytoplankton (2–20 µm) dominate prior and directly after the phytoplankton peak in October and March, respectively (Clarke et al. 2008, Montes-Hugo et al. 2008). The winter phytoplankton community is dominated by nanophytoplankton when phytoplankton biomass is low (<0.02 mg Chl *a* · m⁻³; Clarke et al. 2008). Throughout the year, diatoms form the predominant taxonomic group in the phytoplankton community of northern Marguerite Bay, contributing over 90% of the total biomass during the bloom (Annett et al. 2010, Rozema et al. 2017). The dominance of specific diatom species varies throughout the season and among years, with high relative abundances of genera such as *Fragilariopsis*, *Minidiscus*, *Pseudo-nitzschia*, *Thalassiosira*, *Odontella*, and *Proboscia* (Annett et al. 2010; A. Buma, pers. obs.).

Various laboratory studies have addressed physiological responses of individual Antarctic phytoplankton species to variations in water column conditions such as irradiance (Kropuenske et al. 2009, Arrigo et al. 2010, Mills et al. 2010), nutrients (Van de Poll et al. 2009, Alderkamp et al. 2012, Zhu et al. 2016), and elevated CO₂ (Boelen et al. 2011, Trimbom et al. 2014, Hoppe et al. 2015). However, direct comparisons between different Antarctic phytoplankton species have often been limited to *Phaeocystis antarctica* and a single diatom species (Kropuenske et al. 2009, Arrigo et al. 2010, Alderkamp et al. 2012) and only a few studies have compared the diverse group of Antarctic diatoms in more detail (Karentz et al. 1991, Helbling et al. 1996, Timmermans et al. 2001a,b, Trimbom et al. 2013, 2014, Zhu et al. 2016). Antarctic diatoms are believed to dominate in shallow mixed layers with relatively high irradiance conditions due to effective photoprotection mechanisms, such as flexibility in photosystem II (PSII) connectivity, functional absorption cross section, de-epoxidation of the xanthophyll pigment cycle and consequent non-photochemical quenching (NPQ; Kropuenske et al. 2009, Van de Poll et al. 2011, Boelen et al. 2011, Trimbom et al. 2014). Moreover, Antarctic diatoms are able to photoacclimate to high irradiances by reducing cellular chlorophyll *a* and PSII reaction center abundance and/or antenna size and increasing cellular photoprotective pigmentation or other non-photochemical processes (Kropuenske et al. 2009, 2010, Boelen et al. 2011). Typically, changes in light harvesting capacity are matched by an increase in the amount and/or activity of RUBISCO (Falkowski and La Roche 1991, MacIntyre et al. 1996), although this step is believed to be rate limiting in Antarctic diatoms (Young et al. 2014). Further research on Antarctic diatom species has revealed that smaller diatom species showed higher specific growth rates and thrive under lower irradiance and nutrient conditions compared to larger diatoms species (Karentz et al. 1991, Timmermans et al. 2001a, b). In temperate diatom species this has been attributed to a relatively high light harvesting capacity, higher susceptibility to photoinhibition, but higher nutrient uptake capacity and lower nutrient requirement in smaller compared to larger diatom species (Finkel 2001, Key et al. 2010, Grover 2011). This suggests that smaller diatom species would benefit from low irradiance and nutrient conditions, whereas larger diatoms species might exhibit more efficient photoprotection under the high irradiance conditions prevailing in shallow mixed layers, for example, caused by melt water stratification (Finkel 2001, Montes-Hugo et al. 2008, Key et al. 2010).

Despite the importance of large diatom species such as *Proboscia* and *Thalassiosira* (cell length/diameter >150 µm and/or biovolume >6,000 µm³) during the phytoplankton bloom in Marguerite Bay (Annett et al. 2010, A. Buma, pers. obs.),

experimental photophysiological research has mainly focused on smaller Antarctic diatom species such as *Fragilariopsis* and *Chaetoceros* (cell length <60 μm and/or biovolume <600 μm^3 ; Timmermans et al. 2001a,b, Zhu et al. 2016). Since multiple studies have shown the importance of size scaling in phytoplankton performance (Raven 1998, Finkel 2001, Key et al. 2010), this study addressed the question whether size governs the photophysiological response of diatoms to irradiance conditions found in the coastal WAP. To this end, the following four Antarctic diatom species were freshly isolated in northern Marguerite Bay: *Fragilariopsis* sp., *Pseudo-nitzschia* cf. *subcurvata*, *Thalassiosira* cf. *antarctica*, and *Proboscia* cf. *alata*. These co-occurring diatoms differ in over two orders of magnitude in cell size and biovolume, as well as specific pigment fingerprint, and represent the diverse group of diatoms found in the WAP (Annett et al. 2010; A. Buma, pers. obs.). *Fragilariopsis* sp., *P. subcurvata*, *T. antarctica*, and *P. alata* were acclimated to three different irradiances and photophysiology, electron transport, carbon fixation and growth were assessed. Results are discussed in the context of size scaling and the influence of photoacclimation potential on the success of specific diatom species in natural phytoplankton communities in the coastal Antarctic waters of the WAP.

MATERIALS AND METHODS

Isolation of Antarctic diatom species. The Antarctic diatom species *Fragilariopsis* sp., *Pseudo-nitzschia* cf. *subcurvata*, *Thalassiosira* cf. *antarctica*, and *Proboscia* cf. *alata* were isolated at the long-term RaTS station (67°34.20' S, 68°13.50' W) in northern Marguerite Bay, WAP in January–February 2014. *Fragilariopsis* sp. and *P. subcurvata* were isolated using 10% serial dilutions in f/2 + Si medium based on natural oceanic seawater (Guillard 1975). *Thalassiosira antarctica* and *P. alata* were manually isolated using light microscopy (100–200 \times magnification, Zeiss Axiomat microscope) and sterilized Pasteur pipettes and post isolated using 10% serial dilutions in f/2 + Si medium. Species identification was performed using light microscopy according to Scott and Thomas (2005). Additional analysis of 18S rRNA sequences (MiSeq, Illumina), annotated using the PR² database with curated taxonomy (Guillou et al. 2013), from environmental samples collected at RaTS showed the presence of identical genera (P.D. Rozema, unpub. data). The Antarctic diatom species were subsequently cultivated in f/2 + Si medium in 100 mL glass Erlenmeyer flasks at 10 $\mu\text{mol photons} \cdot \text{m}^{-2} \cdot \text{s}^{-1}$ (Biolux lamps, Osram) in a diurnal cycle of 16:8 h light:dark at 4°C.

Experimental design. Cultures of *Fragilariopsis* sp., *Pseudo-nitzschia subcurvata*, *Thalassiosira antarctica*, and *Proboscia alata* were transferred to 500 mL glass Erlenmeyer flasks and incubated in triplicate ($n = 3$) at 10, 50, and 100 $\mu\text{mol photons} \cdot \text{m}^{-2} \cdot \text{s}^{-1}$. The three experimental irradiances were provided as a square wave function with a 16:8 h light:dark cycle in a U-shaped lamp setup (for details see Van de Poll et al. 2007). The irradiance levels in the setup were frequently monitored using a QSL-2101 (Biospherical Instruments, Santa Clara, CA, USA). The temperature in the setup was maintained at 1°C by a thermostat (RK 8 KS, edition 2000; Lauda Dr. R. Wobser & Co., Lauda-Königshofen,

Germany) and deviated less than $\pm 0.5^\circ\text{C}$. After an acclimation period of 14 d under the experimental irradiance and temperature conditions, cultures of the four diatom species were transferred to fresh f/2 + Si medium to start the experiment. During the experiment, growth and maximum quantum yield of PSII (F_v/F_m) were followed daily starting directly after the beginning of the incubation. In the mid-exponential growth phase ($t = 6\text{--}14$ d), cellular characteristics of the cultures were assessed by the analysis of cell size, biovolume, and cellular carbon, photophysiology was assessed by the analysis of pigments, absorption spectra, F_v/F_m , and NPQ, and photosynthetic rates were assessed by the analysis of electron transport rates (ETR) and carbon fixation rates.

Growth measurements. Samples for cell counts were collected daily during the exponential growth phase. Duplicate samples (2 mL) of each replicate culture were fixed using lugol (0.04% final concentration) and formaline (0.04% final concentration) and cell concentrations were determined by light microscopy (Standard WL; Zeiss, Oberkochen, Germany) according to LeGresley and McDermott (2010) using an improved Neubauer counting chamber for *Fragilariopsis* sp. and a Sedgewick-Rafter counting chamber for *Pseudo-nitzschia subcurvata*, *Thalassiosira antarctica* and *Proboscia alata*. Growth rates ($\mu \cdot \text{d}^{-1}$) of the exponential growth phase were calculated by linear regression of natural log-transformed cell numbers for all replicates (≥ 4 data points).

In addition to cell counts, cell dimensions were measured in samples collected in the mid-exponential growth phase for each replicate culture using light microscopy (Standard WL; Zeiss). Following Hillebrand et al. (1999), cell dimensions ($n = 75$) were estimated by the measurement of the apical, transapical, and perivalvar axis (cell length, width, and height, respectively) for *Fragilariopsis* sp. and *Pseudo-nitzschia subcurvata* and by the cell diameter and height for *Thalassiosira antarctica* and *Proboscia alata*. Measurements of cell dimensions were then used to calculate biovolume, cell surface, and surface-to-volume (S/V) ratios according to Hillebrand et al. (1999).

Cellular carbon. Samples for particulate organic carbon (POC) analysis were taken during the mid-exponential growth phase for each replicate culture. Duplicate samples (15–30 mL) were filtered onto precombusted (4 h, 600°C) 12 mm GF/F filters (Whatman, Maidstone, United Kingdom), snap frozen in liquid nitrogen, and stored at -80°C until further analysis. For analysis, filters were acidified under HCl (37%) fumes for 4 h, dried overnight at 60°C, and wrapped in tin capsules (Elemental Microanalysis Ltd., Okehampton, United Kingdom). Analysis of the samples was performed on a cavity ring-down spectrometer type G2101-I (Picarro, Santa Clara, CA, USA) with a combustion module (Costech, Santa Clara, CA, USA).

Pigment composition. Samples for pigment analysis were taken during the mid-exponential growth phase for each replicate culture. Samples (15–60 mL) were filtered onto 25 mm GF/F filters (Whatman), snap frozen in liquid nitrogen and stored at -80°C until further analysis. Pigments were quantified using high-performance liquid chromatography (HPLC) as described by Van Heukelem and Thomas (2001) and modified according to Perl (2009). In short, filters were freeze-dried for 48 h and pigments were immediately extracted in 3 mL 90% acetone (v/v, 48 h, 4°C). Detection of pigments was carried out using a HPLC (Waters 2695 separation module, 996 photodiode array detector) equipped with a Zorbax Eclipse extra dense bonding C₈ 3.5 μm column (Agilent Technologies, Santa Clara, CA, USA). Peaks were identified by retention time and diode array spectroscopy. Pigments were quantified using standard dilutions (DHI LAB products) of chlorophyll *a* (Chl *a*), chlorophyll *c*₂ (Chl-*c*₂) chlorophyll *c*₃ (Chl-*c*₃), fucoxanthin (Fuco), diadinoxanthin (Dd), diatoxanthin (Dt), and β -carotene (β -car). The de-epoxidation state (DPS) of the xanthophyll pigment cycle was calculated as $\text{Dt}/(\text{Dd} + \text{Dt})$.

Absorption spectra. Samples for pigment absorption spectra were taken during the mid-exponential growth phase for each replicate culture. Phytoplankton pigment absorption spectra were determined on a Cary 3E UV-Vis spectrophotometer (Varian, CA, USA), equipped with an integrating sphere. Spectral values of the absorption coefficient were recorded every 1 nm between 300 and 800 nm. For analysis, 20–60 mL culture sample was filtered onto 25 mm GF/F filters (Whatman) and the transmission and reflection of the total particulate matter was determined according to Tassan and Ferrari (1995). The filter was then extracted in sodium hypochlorite (1% chlorine) to remove phytoplankton pigments and measured again to obtain the absorption of non-pigmented material (detritus). Phytoplankton absorption was calculated and normalized to Chl *a* concentrations to obtain the specific absorption coefficient by phytoplankton $a^*_{ph}(\lambda)$ ($m^2 \cdot mg \text{ Chl } a^{-1}$). The irradiance used in the photosynthetron during carbon fixation measurements was used to obtain the spectrally weighted mean specific absorption coefficient \bar{a}^* ($m^2 \cdot \mu g \text{ Chl } a^{-1}$) between 400 and 700 nm.

PSII chlorophyll fluorescence characteristics. PSII fluorescence analyses were performed on a pulse amplitude modulation (PAM) chlorophyll fluorometer (Waltz GmbH, Bad Waldsee, Germany) equipped with a WATER emitter-detector (ED) unit and analyzed using WinControl software (version 2.08; Waltz GmbH) according to Maxwell and Johnson (2000) (and references therein) and Kulk et al. (2012, 2013). For daily analysis, 10 mL samples were dark adapted for 20 min at 1°C. Then, F_0 was recorded as the minimal fluorescence and F_m^0 as the maximum fluorescence in the dark-adapted state. F_v/F_m was calculated as $(F_m^0 - F_0)/F_m^0$.

In addition to the daily analysis of F_v/F_m , NPQ and ETR were assessed in the mid-exponential growth phase. Both measurements were performed in a climate controlled room at 1°C that deviated less than $\pm 0.5^\circ\text{C}$. For measurements of NPQ, 10 mL samples were dark adapted for 20 min at 1°C, after which the F_v/F_m was recorded as described above. Samples were then exposed to high irradiance ($456 \mu\text{mol photons} \cdot m^{-2} \cdot s^{-1}$ provided by a blue led at 460 nm) for 5 min after which the quantum yield of PSII (Φ_{PSII}) was determined every 5 min during a recovery period of 1 h by measuring F_t as the steady-state fluorescence prior to the saturating light flash and F_m' as the maximum fluorescence in the light. Φ_{PSII} was calculated as $(F_m' - F_t)/F_m'$. From the F_v/F_m measurements at $t = 0$ min and the Φ_{PSII} measurements at $t = 5$ min, total NPQ was calculated as $(F_m^0 - F_m')/F_m'$. Relaxation analysis was performed to calculate the contribution of slowly and fast relaxing NPQ to estimate photoinhibition and photoprotection, respectively. (Walters and Horton 1991, Osmond 1994, Maxwell and Johnson 2000). To this end, F_m' values were corrected for F_0 and extrapolated to estimate the value of F_m' that would have been attained if only slowly relaxing quenching was present in the light (F_m^r). Slowly relaxing non-photochemical quenching (NPQ_s) was then calculated as $(F_m^0 - F_m^r)/F_m^r$ and fast relaxing non-photochemical quenching (NPQ_f) as $(F_m^0/F_m') - (F_m^0 - F_m^r)$.

For measurements of ETR, duplicate 10 mL samples were dark adapted for 20 min at 1°C. The F_v/F_m was recorded at $0 \mu\text{mol photons} \cdot m^{-2} \cdot s^{-1}$ and the Φ_{PSII} was recorded after 1 min exposure to 7 different irradiance levels ranging from 8 to $456 \mu\text{mol photons} \cdot m^{-2} \cdot s^{-1}$ provided by the actinic light of the WATER-PAM (blue led, 460 nm). The absolute ETR (ETR in $\text{mol } e^- \cdot \mu g \text{ Chl } a^{-1} \cdot h^{-1}$) for each irradiance level was calculated by $\Phi_{PSII} \times E \times \bar{a}^* \times 0.5$, where E ($\mu\text{mol photons} \cdot m^{-2} \cdot s^{-1}$) is the irradiance level of the WATER-PAM, \bar{a}^* ($m^2 \cdot mg \text{ Chl } a^{-1}$) is the spectrally weighted mean specific absorption coefficient, and 0.5 is a factor accounting for the partitioning of energy between photosystem I (PSI) and PSII. ETR versus irradiance curves were fitted to the

empirical model described by Platt et al. (1980) using MatLab software (version 8.3; Mathworks, Natick, MA, USA) to estimate the maximum electron transport rate (ETR_{max} in $\text{mol } e^- \cdot \mu g \text{ Chl } a^{-1} \cdot h^{-1}$), the initial slope of electron transport (α_{ETR} in $\text{mol } e^- \cdot \mu g \text{ Chl } a^{-1} \cdot h^{-1}$ ($\mu\text{mol photons} \cdot m^{-2} \cdot s^{-1}$)⁻¹), and the photoacclimation index of electron transport (EK_{ETR} in $\mu\text{mol photons} \cdot m^{-2} \cdot s^{-1}$).

Carbon fixation. Samples for carbon fixation rates were taken during the mid-exponential growth phase for each replicate culture. A ¹⁴C-bicarbonate method was used to determine photosynthetic versus irradiance (PE) characteristics as described by Lewis and Smith (1983) and Kulk et al. (2011). In short, 17 vials with 2 mL radiolabeled culture samples (0.74 MBq total activity ¹⁴C-bicarbonate) were incubated for 60 min at 1°C in a photosynthetron consisting of a temperature controlled aluminum block illuminated by a 250 W lamp (HCI-TT 250W/942 NDL PB power ball; Osram, München, Germany) with irradiance levels ranging from 4 to $1,158 \mu\text{mol photons} \cdot m^{-2} \cdot s^{-1}$. Time zero activity and total activity were determined for each PE measurement. Radioactivity in all samples was measured by liquid scintillation spectrometry (Tri-Carb 2000 CA scintillation counter; Packard, MA, USA) using 10 mL Ultima Gold XR scintillation cocktail (PerkinElmer, MA, USA). Data from the PE measurements were normalized to Chl *a* derived from HPLC measurements and fitted to the empirical model described by Platt et al. (1980) using MatLab software (version 8.3; Mathworks) to estimate the maximum carbon fixation rate (P_{max} in $\mu g \text{ C} \cdot \mu g \text{ Chl } a^{-1} \cdot h^{-1}$), the initial slope of carbon fixation (α in $\mu g \text{ C} \cdot \mu g \text{ Chl } a^{-1} \cdot h^{-1}$ [$\mu\text{mol photons} \cdot m^{-2} \cdot s^{-1}$]⁻¹), the photoacclimation index (EK in $\mu\text{mol photons} \cdot m^{-2} \cdot s^{-1}$), and photoinhibition of carbon fixation (β in $\mu g \text{ C} \cdot \mu g \text{ Chl } a^{-1} \cdot h^{-1}$ [$\mu\text{mol photons} \cdot m^{-2} \cdot s^{-1}$]⁻¹). The electron requirement of carbon fixation ($\Phi_{e,C}$ in $\text{mol } e^- \cdot \text{mol C}^{-1}$) was calculated using the ETR and carbon fixation measurements normalized to Chl *a*. PE measurements were also normalized to cellular C (data not shown), which yielded similar results in size scaling compared to Chl *a* normalized measurements.

Statistical analysis. Differences between the irradiance conditions and the diatom species were statistically tested by ANOVA and Tukey HSD post hoc analysis using STATISTICA software (version 13.0; Statsoft, TX, USA). Before analysis, data were tested for normality and homogeneity of variances and log transformed for further statistical analysis when necessary. Differences were considered significant when $P < 0.05$.

To analyze the role of cell size on growth, photophysiology, and photosynthetic rates, size scaling exponents (SSE) were determined according to Peters (1983). To this end, all parameters were log transformed and linear regression analysis was performed using Sigmaplot software (version 11; Systat Software Inc., San Jose, California, United States of America) to determine the SSE and intercept for each parameter on the basis of biovolume. Additional analysis on the basis of S/V ratios showed similar results (data not shown). Regression coefficients were considered significant within 95% confidence intervals.

RESULTS

Growth. Growth rates varied widely among irradiance conditions and diatoms (Fig. 1). Growth rates increased with increasing irradiance in *Fragilariopsis* sp., *Pseudo-nitzschia subcurvata*, and *Thalassiosira antarctica* ($F_{2,23} = 32.3$, $P < 0.05$). In contrast, in *Pro-boscia alata*, growth rates increased from 10 to $50 \mu\text{mol photons} \cdot m^{-2} \cdot s^{-1}$, but decreased at the highest irradiance of $100 \mu\text{mol photons} \cdot m^{-2} \cdot s^{-1}$ ($F_{2,23} = 32.3$, $P < 0.001$). Highest growth rates were

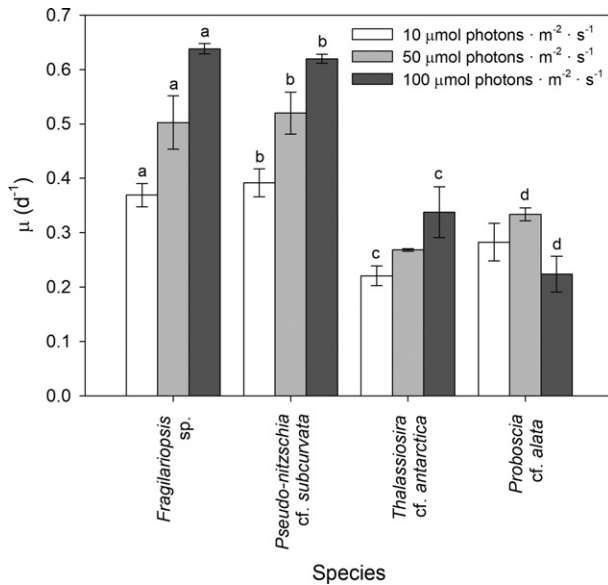


FIG. 1. Mean (\pm SD, $n = 3$) growth rates (μ in d^{-1}) are given for the four Antarctic diatom species *Fragilariopsis* sp. (*Fragilariopsis* sp.), *Pseudo-nitzschia* cf. *subcurvata* (Ps), *Thalassiosira* cf. *antarctica* (Ta), and *Proboscia* cf. *alata* (Pa) grown at 10, 50, and 100 $\mu\text{mol photons} \cdot \text{m}^{-2} \cdot \text{s}^{-1}$. Significant differences ($P < 0.05$) between the different irradiance conditions for each diatom species are indicated by identical letters.

found in the smaller species *Fragilariopsis* sp. and *Pseudo-nitzschia subcurvata*, ranging from 0.37 ± 0.021 to $0.64 \pm 0.009 \cdot \text{d}^{-1}$ and 0.39 ± 0.026 to $0.62 \pm 0.008 \cdot \text{d}^{-1}$, respectively ($F_{3,23} = 129$, $P < 0.05$). Lowest growth rates were found in the larger species *Thalassiosira antarctica* and *Proboscia alata* with growth rates ranging from 0.22 ± 0.018 to $0.27 \pm 0.002 \cdot \text{d}^{-1}$ and 0.22 ± 0.033 to $0.33 \pm 0.012 \cdot \text{d}^{-1}$, respectively ($F_{3,23} = 129$, $P < 0.05$). Calculations of SSE showed a negative relationship between biovolume and growth, which increased with irradiance (Table 1).

Cell size and biovolume. The four Antarctic diatom species varied greatly in cell shape, cell size, biovolume, and S/V ratios. Irradiance had no effect on cell length, biovolume, and S/V ratios in *Fragilariopsis* sp. and *Thalassiosira antarctica* (Table 2). In *Pseudo-nitzschia subcurvata*, cell length and biovolume increased at higher irradiances ($F_{2,6} = 13.1$, $F_{2,6} = 12.6$, $P < 0.05$), whereas the S/V ratio was highest at 50 $\mu\text{mol photons} \cdot \text{m}^{-2} \cdot \text{s}^{-1}$ ($F_{2,6} = 15.8$, $P < 0.01$). A contrasting trend was observed in *Proboscia alata*, with a decrease in cell length and biovolume and an increase in the S/V ratio at higher irradiances ($F_{2,6} = 14.0$, $F_{2,6} = 161$, $F_{2,6} = 1.44$, $P < 0.05$). *Fragilariopsis* sp. was the smallest species with significantly shortest (apical) cell length and smallest biovolume, followed by *P. subcurvata*, *T. antarctica*, and *P. alata*, respectively ($F_{2,32} = 530$, $F_{2,32} = 198$, $P < 0.05$; Table 2). Cell length and biovolume between the smallest species *Fragilariopsis* sp. and the largest species *P. alata* varied approximately two orders of

magnitude. Related to cell dimensions and biovolume, *Fragilariopsis* sp. showed highest S/V ratios, followed by *Pseudo-nitzschia subcurvata*, *Proboscia alata*, and *Thalassiosira antarctica*, respectively ($F_{2,32} = 5,508$, $P < 0.001$; Table 2).

Cellular carbon. Irradiance had no effect on cellular carbon concentrations in *Fragilariopsis* sp. and *Proboscia alata*, whereas concentrations decreased at 100 $\mu\text{mol photons} \cdot \text{m}^{-2} \cdot \text{s}^{-1}$ in *Pseudo-nitzschia subcurvata* ($F_{2,5} = 8.74$, $P < 0.05$) and increased at 50 and 100 $\mu\text{mol photons} \cdot \text{m}^{-2} \cdot \text{s}^{-1}$ in *Thalassiosira antarctica* ($F_{2,6} = 30.7$, $P < 0.01$; data not shown). Cellular carbon was highly related to cell size and biovolume with lowest concentrations found in the smaller species *Fragilariopsis* sp. ($5.32 \pm 1.42 \text{ pg C} \cdot \text{cell}^{-1}$) and highest concentrations found in the larger species *P. alata* ($1,129 \pm 289 \text{ pg C} \cdot \text{cell}^{-1}$; data not shown). The positive relationship between biovolume and cellular carbon was also evident in the SSE, at all irradiances (Table 1).

C:Chl *a* increased with irradiance in all diatom species ($F_{2,24} = 4.09$, $P < 0.05$, not significant for *Proboscia alata*; Table 3) and was related to a significant decrease in cellular Chl *a*. When the four diatoms were compared, *Fragilariopsis* sp. and *Pseudo-nitzschia subcurvata* showed highest C:Chl *a* at higher irradiances, *P. alata* showed highest C:Chl *a* at 10 $\mu\text{mol photons} \cdot \text{m}^{-2} \cdot \text{s}^{-1}$ ($F_{3,24} = 4.02$, $P < 0.05$) and *Thalassiosira antarctica* showed overall lowest C:Chl *a* (Table 3). The SSE showed a similar trend with a negative relationship between biovolume and C:Chl *a* at 50 and 100 $\mu\text{mol photons} \cdot \text{m}^{-2} \cdot \text{s}^{-1}$ and no relationship at the lowest irradiance (Table 1).

Pigment composition. The major pigments chlorophyll *a*, chlorophyll *c*₂, diadinoxanthin, diatoxanthin, fucoxanthin, and β -carotene were present in all four Antarctic diatom species (Fig. 2, Table 3). The pigment composition of *Pseudo-nitzschia subcurvata* and *Proboscia alata* was further characterized by the presence of chlorophyll *c*₃ (Fig. 2). Cellular Chl *a* concentrations significantly decreased with increasing irradiance in *Fragilariopsis* sp., *P. subcurvata* and *P. alata* ($F_{2,22} = 6.44$, $P < 0.05$), whereas no changes were observed in *Thalassiosira antarctica* (Table 3). Cellular Chl *a* was highly related to size with lowest concentrations found in *Fragilariopsis* sp. and highest concentrations found in *T. antarctica* and *P. alata* (Table 3). Calculations of SSE also showed a positive relationship between biovolume and Chl *a*, which increased with irradiance (Table 1).

The concentration and activity of xanthophyll pigments showed a strong, uniform response to increasing irradiances in all species (Figs. 2 and 3). Both cellular Dd and Dd/Chl *a* increased from 10 to 50 $\mu\text{mol photons} \cdot \text{m}^{-2} \cdot \text{s}^{-1}$ ($F_{2,22} = 141$, $P < 0.05$), but did not increase further at 100 $\mu\text{mol photons} \cdot \text{m}^{-2} \cdot \text{s}^{-1}$. Cellular Dt and Dt/Chl *a* significantly increased at higher irradiances with highest concentrations found at 100 $\mu\text{mol photons} \cdot \text{m}^{-2} \cdot \text{s}^{-1}$ ($F_{2,22} = 148$, $P < 0.05$). In addition, the DPS of the xanthophyll pigment cycle significantly increased at higher irradiances, with the

TABLE 1. Size scaling exponent and intercept (\pm SD, $n = 12$) are given for growth (μ), cellular carbon (C), carbon to chlorophyll a ratio (C:Chl a), cellular chlorophyll a (Chl a), specific absorption cross section (\bar{a}^*), maximum quantum yield of PSII (F_v/F_m), non-photochemical quenching (NPQ), slowly relaxing non-photochemical quenching (NPQ_s), fast relaxing non-photochemical quenching (NPQ_f), maximum electron transport rate (ETR_{max}), initial slope of electron transport (α_{ETR}), photoacclimation index of electron transport (E_KETR), maximum carbon fixation rate (P_{max}), initial slope of carbon fixation (α), photoacclimation index of carbon fixation (E_K), photoinhibition of carbon fixation (β), and electron requirement of carbon fixation ($\Phi_{e,C}$) at 10, 50 and 100 $\mu\text{mol photons} \cdot \text{m}^{-2} \cdot \text{s}^{-1}$. Significant regression coefficients within 95% confidence intervals are indicated by * and within 99% confidence intervals by **.

	10 $\mu\text{mol photons} \cdot \text{m}^{-2} \cdot \text{s}^{-1}$			50 $\mu\text{mol photons} \cdot \text{m}^{-2} \cdot \text{s}^{-1}$			100 $\mu\text{mol photons} \cdot \text{m}^{-2} \cdot \text{s}^{-1}$		
	Scaling exponent	Intercept	r^2	Scaling exponent	Intercept	r^2	Scaling exponent	Intercept	r^2
μ	-0.070 ± 0.0152	-0.32 ± 0.045	0.679**	-0.092 ± 0.0143	-0.16 ± 0.042	0.806**	-0.142 ± 0.0265	-0.02 ± 0.077	0.742**
C	0.772 ± 0.0202	-0.10 ± 0.060	0.993**	0.822 ± 0.0127	-0.18 ± 0.038	0.998**	0.860 ± 0.0316	-0.35 ± 0.092	0.989**
C:Chl a	0.004 ± 0.0241	1.44 ± 0.072	0.003	-0.037 ± 0.0149	1.71 ± 0.044	0.383*	-0.077 ± 0.0155	1.89 ± 0.045	0.755**
Chl a	0.767 ± 0.0243	-1.54 ± 0.073	0.990**	0.859 ± 0.0148	-1.89 ± 0.044	0.997**	0.936 ± 0.0387	-2.24 ± 0.112	0.987**
\bar{a}^*	-0.024 ± 0.0193	-1.65 ± 0.058	0.135	-0.070 ± 0.0248	-1.51 ± 0.073	0.443*	-0.074 ± 0.0232	-1.44 ± 0.067	0.558*
F_v/F_m	0.009 ± 0.0052	-0.23 ± 0.016	0.247	0.007 ± 0.0038	-0.26 ± 0.011	0.240	-0.017 ± 0.0083	-0.25 ± 0.024	0.299
NPQ	0.046 ± 0.0178	0.41 ± 0.053	0.399*	-0.013 ± 0.0236	0.71 ± 0.070	0.030	-0.038 ± 0.0292	0.67 ± 0.085	0.177
NPQ _s	0.137 ± 0.0557	-0.80 ± 0.166	0.377*	0.122 ± 0.0396	-0.76 ± 0.117	0.487*	0.142 ± 0.0756	-1.01 ± 0.219	0.306
NPQ _f	0.032 ± 0.0159	0.40 ± 0.047	0.285	-0.028 ± 0.0264	0.71 ± 0.078	0.103	-0.054 ± 0.0275	0.67 ± 0.080	0.323
ETR _{max}	0.122 ± 0.0345	-1.17 ± 0.103	0.555**	-0.019 ± 0.0301	-0.61 ± 0.089	0.040	-0.032 ± 0.0417	2.57 ± 0.204	0.069
α_{ETR}	0.036 ± 0.0365	-2.60 ± 0.109	0.087	-0.075 ± 0.0254	-2.26 ± 0.075	0.467*	-0.063 ± 0.0141	-0.35 ± 0.092	0.714**
E _K ETR	0.086 ± 0.0268	1.43 ± 0.080	0.508**	0.056 ± 0.0258	1.65 ± 0.076	0.320	0.031 ± 0.0408	1.89 ± 0.045	0.068
P_{max}	0.021 ± 0.0310	0.23 ± 0.093	0.044	-0.070 ± 0.0394	0.53 ± 0.117	0.240	-0.066 ± 0.0285	0.74 ± 0.085	0.399
α	-0.130 ± 0.0408	-0.76 ± 0.122	0.502**	-0.108 ± 0.0317	-0.85 ± 0.094	0.537**	-0.053 ± 0.0180	-1.04 ± 0.075	0.515*
E _K	0.150 ± 0.0656	0.99 ± 0.196	0.345*	0.038 ± 0.0539	1.38 ± 0.160	0.047	-0.025 ± 0.0273	1.82 ± 0.079	0.093
β	-0.066 ± 0.0826	-2.90 ± 0.247	0.059	0.087 ± 0.0714	-3.37 ± 0.212	0.129	-0.059 ± 0.0519	-2.69 ± 0.151	0.139
$\Phi_{e,C}$	-0.121 ± 0.0310	1.78 ± 0.093	0.602**	-0.010 ± 0.0178	1.22 ± 0.053	0.033	-0.008 ± 0.0270	1.23 ± 0.078	0.011

TABLE 2. Mean (\pm SD, $n = 3$) cell length (μm), biovolume (μm^3) and cell surface to volume ratio (S/V in μm^{-1}) are given for the four Antarctic diatom species *Fragilariopsis* sp., *Pseudo-nitzschia* cf. *subcurvata*, *Thalassiosira* cf. *antarctica*, and *Proboscica* cf. *alata* grown at 10, 50, and 100 $\mu\text{mol photons} \cdot \text{m}^{-2} \cdot \text{s}^{-1}$. Cell length is given as the (apical) length for *Fragilariopsis* sp. and *P. subcurvata*, as the cell height for *P. alata* and as the diameter for *T. antarctica*. Significant differences ($P < 0.05$) between the different irradiance conditions for each diatom species are indicated by matching letters.

	<i>Fragilariopsis</i> sp.	<i>Pseudo-nitzschia</i> cf. <i>subcurvata</i>	<i>Thalassiosira</i> cf. <i>antarctica</i>	<i>Proboscica</i> cf. <i>alata</i>
Cell length				
10	$3.56 \pm 2.00 \times 10^{-2}$	28.6 ± 2.59^a	24.2 ± 0.13	$271 \pm 6.11^{c,d}$
50	$3.50 \pm 2.00 \times 10^{-2}$	30.1 ± 1.89^b	23.8 ± 0.39	220 ± 21.4^c
100	$3.54 \pm 6.00 \times 10^{-2}$	$36.1 \pm 0.73^{a,b}$	23.4 ± 0.24	220 ± 8.15^d
Biovolume				
10	14.6 ± 1.58	77 ± 8.48^a	$6,646 \pm 57$	$10,543 \pm 93^b$
50	13.9 ± 1.01	93 ± 7.11	$6,657 \pm 359$	$8,310 \pm 477^b$
100	14.2 ± 0.23	103 ± 0.93^a	$6,288 \pm 267$	$6,360 \pm 92^b$
S/V				
10	$2.32 \pm 9.41 \times 10^{-2}$	$1.16 \pm 3.31 \times 10^{-2a}$	$0.30 \pm 6.28 \times 10^{-4}$	$0.59 \pm 9.01 \times 10^{-3c}$
50	$2.36 \pm 6.86 \times 10^{-2}$	$1.06 \pm 1.01 \times 10^{-2a,b}$	$0.30 \pm 5.58 \times 10^{-3}$	$0.60 \pm 2.19 \times 10^{-2d}$
100	$2.34 \pm 8.22 \times 10^{-3}$	$1.13 \pm 8.89 \times 10^{-3b}$	$0.31 \pm 5.28 \times 10^{-3}$	$0.69 \pm 1.10 \times 10^{-2c,d}$

TABLE 3. Mean (\pm SD, $n = 3$) cellular chlorophyll *a* (Chl *a* in $\text{pg} \cdot \text{cell}^{-1}$), carbon to chlorophyll *a* ratio (Chl *a*:C), maximum photosynthetic yield of PSII (F_v/F_m), and specific absorption cross section (\bar{a}^* in $\text{m}^2 \cdot \text{mg Chl } a^{-1}$) are given for the four Antarctic diatom species *Fragilariopsis* sp., *Pseudo-nitzschia* cf. *subcurvata*, *Thalassiosira* cf. *antarctica*, and *Proboscica* cf. *alata* grown at 10, 50, and 100 $\mu\text{mol photons} \cdot \text{m}^{-2} \cdot \text{s}^{-1}$. Significant differences ($P < 0.05$) between the different irradiance conditions for each diatom species are indicated by identical letters.

	<i>Fragilariopsis</i> sp.	<i>Pseudo-nitzschia</i> cf. <i>subcurvata</i>	<i>Thalassiosira</i> cf. <i>antarctica</i>	<i>Proboscica</i> cf. <i>alata</i>
Chl <i>a</i>				
10 $\mu\text{mol photons} \cdot \text{m}^{-2} \cdot \text{s}^{-1}$	$0.190 \pm 0.032^{a,b}$	1.027 ± 0.163^c	28.79 ± 1.501	29.41 ± 5.801^d
50 $\mu\text{mol photons} \cdot \text{m}^{-2} \cdot \text{s}^{-1}$	0.121 ± 0.016^a	0.648 ± 0.064^c	28.03 ± 0.968	26.41 ± 3.603
100 $\mu\text{mol photons} \cdot \text{m}^{-2} \cdot \text{s}^{-1}$	0.088 ± 0.030^b	0.284 ± 0.046^c	24.06 ± 3.287	19.94 ± 1.136^d
C:Chl <i>a</i>				
10	30.1 ± 2.39^a	$26.3 \pm 1.45^{b,c}$	$21.8 \pm 1.22^{d,e}$	38.2 ± 5.37
50	44.7 ± 3.72^a	46.9 ± 2.77^b	32.1 ± 1.24^d	41.9 ± 6.34
100	61.5 ± 4.87^a	57.0 ± 8.03^c	35.5 ± 4.09^e	45.3 ± 1.50
F_v/F_m				
10	$0.600 \pm 2.09 \times 10^{-3a}$	$0.618 \pm 8.33 \times 10^{-3b}$	$0.685 \pm 1.67 \times 10^{-2c}$	$0.606 \pm 8.77 \times 10^{-3d}$
50	$0.554 \pm 1.31 \times 10^{-3a}$	$0.562 \pm 1.97 \times 10^{-3b}$	$0.606 \pm 1.05 \times 10^{-2c}$	$0.554 \pm 2.43 \times 10^{-3d}$
100	$0.518 \pm 2.68 \times 10^{-2a}$	$0.535 \pm 3.60 \times 10^{-3b}$	$0.519 \pm 7.99 \times 10^{-3c}$	$0.437 \pm 6.87 \times 10^{-3d}$
\bar{a}^*				
10	$0.020 \pm 1.73 \times 10^{-3a}$	$0.022 \pm 7.89 \times 10^{-4}$	$0.014 \pm 1.43 \times 10^{-3}$	$0.022 \pm 6.36 \times 10^{-4}$
50	$0.025 \pm 5.45 \times 10^{-3}$	$0.025 \pm 1.31 \times 10^{-3}$	$0.013 \pm 1.48 \times 10^{-3}$	$0.021 \pm 4.18 \times 10^{-3}$
100	$0.030 \pm 5.85 \times 10^{-3a}$	$0.026 \pm 2.30 \times 10^{-3}$	$0.016 \pm 1.13 \times 10^{-3}$	$0.025 \pm 2.74 \times 10^{-4}$

strongest increase observed in *Pseudo-nitzschia subcurvata* (Fig. 3). No differences in xanthophyll pigment ratios were observed between the four diatoms and *Fragilariopsis* sp., *Pseudo-nitzschia subcurvata*, *Thalassiosira antarctica*, and *Proboscica alata* showed similar Dd/Chl *a* and Dt/Chl *a* (Fig. 2). Cellular concentrations of the xanthophyll pigments had similar SSE as Chl *a*, whereas no relationship with biovolume was observed for Dd/Chl *a*, Dt/Chl *a* and/or the DPS of the xanthophyll pigment cycle (data not shown).

Irradiance also affected the concentrations of other accessory pigments, with a decrease in Chl *c*₂/*a* and Chl *c*₃/*a* at higher irradiances ($F_{2,22} = 46.6$, $F_{2,22} = 78.7$, $P < 0.05$) in all species. Moreover, Fuco/Chl *a* decreased at higher irradiances in *Pseudo-nitzschia subcurvata* and *Proboscica alata* ($F_{2,22} = 94.3$, $P < 0.05$), but was not affected by irradiance in *Fragilariopsis* sp. and *Thalassiosira antarctica* (Fig. 2). When the four diatoms were compared, Chl *c*₂/*a* and Fuco/

Chl *a* were higher in *Fragilariopsis* sp., *P. subcurvata* and *P. alata* (ranging between 0.113–0.196 and 0.473–0.785, respectively) compared to *T. antarctica* (ranging from 0.057–0.069 and 0.449–0.472, respectively; $F_{3,22} = 180$, $F_{3,22} = 298$, $P < 0.05$; Fig. 2). In addition, Chl *c*₂/*a* was lower in *P. subcurvata* (0.002–0.037) compared to *P. alata* (0.137–0.186; $F_{3,22} = 1,505$, $P < 0.001$; Fig. 2). The SSE of cellular concentrations of the accessory pigments were similar to those of Chl *a*, whereas no relationship with biovolume was observed for ratios per Chl *a* (data not shown).

Absorption spectra. Absorption characteristics varied among irradiance conditions and diatoms. In *Fragilariopsis* sp., \bar{a}^* increased with increasing irradiances ($F_{2,22} = 5.97$, $P < 0.05$) and a similar, but not significant trend was observed in the other species (Table 3). \bar{a}^* was lower in *Thalassiosira antarctica* compared to the other Antarctic diatom species ($F_{3,22} = 23.5$, $P < 0.05$), whereas *Fragilariopsis* sp.,

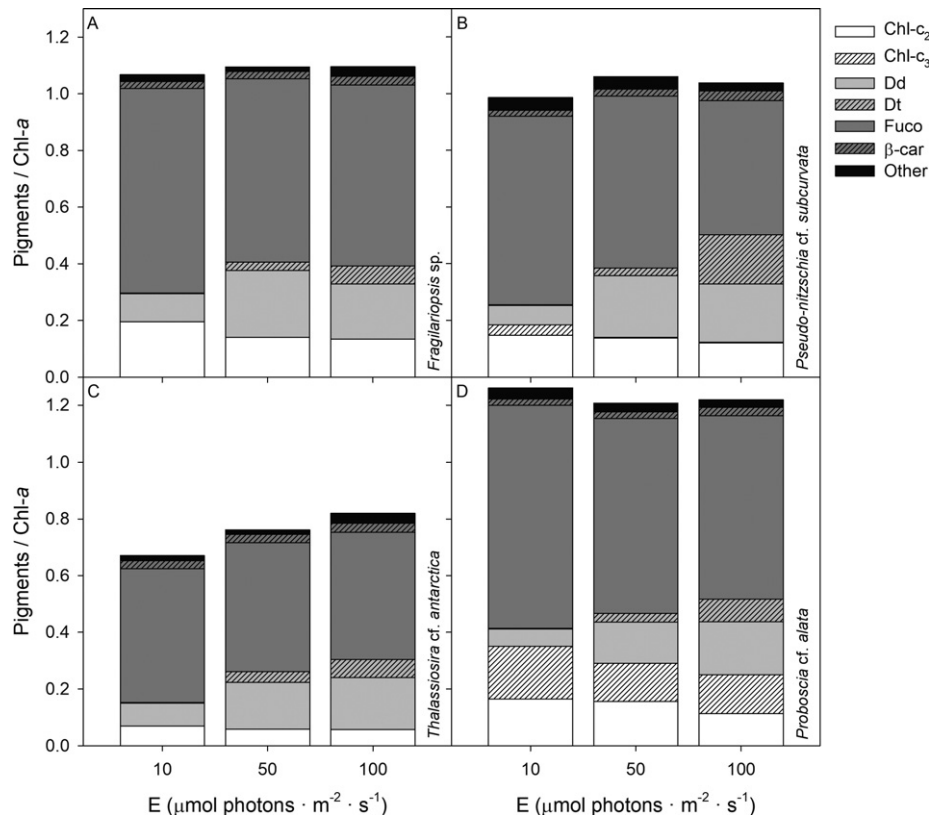


FIG. 2. Mean ($n = 3$) pigment compositions are given for the four Antarctic diatom species (A) *Fragilariopsis* sp., (B) *Pseudo-nitzschia* cf. *subcurvata*, (C) *Thalassiosira* cf. *antarctica*, and (D) *Proboscia* cf. *alata* grown at 10, 50, and 100 $\mu\text{mol photons} \cdot \text{m}^{-2} \cdot \text{s}^{-1}$. Identified pigments (given as ratio per chlorophyll *a* (Chl *a*)) included chlorophyll c_2 (Chl- c_2), chlorophyll c_3 (Chl- c_3), diadinoxanthin (Dd), diatoxanthin (Dt), fucoxanthin (fuco), β -carotene (β -car) and other identified pigments ($<2.5\%$ of total).

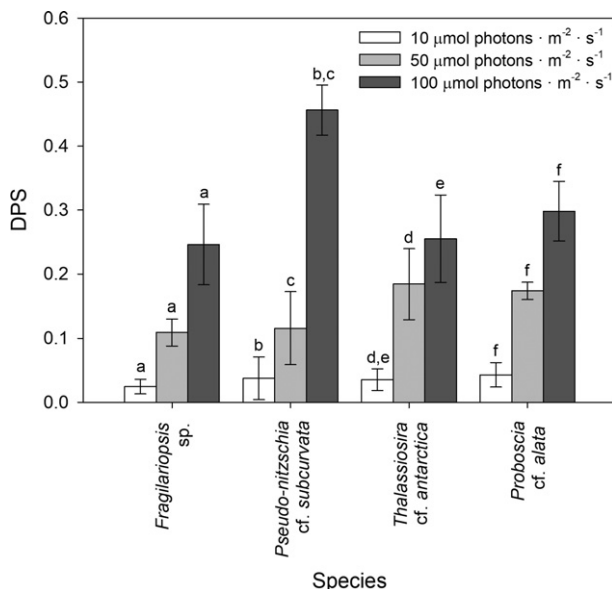


FIG. 3. Mean (\pm SD, $n = 3$) de-epoxidation state (DPS) of the xanthophyll pigment cycle is given for the four Antarctic diatom species *Fragilariopsis* sp. (*Fragilariopsis* sp.), *Pseudo-nitzschia* cf. *subcurvata* (Ps), *Thalassiosira* cf. *antarctica* (Ta), and *Proboscia* cf. *alata* (Pa) grown at 10, 50, and 100 $\mu\text{mol photons} \cdot \text{m}^{-2} \cdot \text{s}^{-1}$. Significant differences ($P < 0.05$) between the different irradiance conditions for each diatom species are indicated by identical letters.

Pseudo-nitzschia subcurvata, and *Proboscia alata* showed similar absorption characteristics (Fig. 4, Table 3). The SSE of \bar{a}^* showed a negative relationship with biovolume at 50 and 100 $\mu\text{mol photons} \cdot \text{m}^{-2} \cdot \text{s}^{-1}$, whereas no relationship with biovolume was observed at 10 $\mu\text{mol photons} \cdot \text{m}^{-2} \cdot \text{s}^{-1}$ (Table 1).

PSII chlorophyll fluorescence characteristics. F_v/F_m decreased with increasing irradiances in all diatom species ($F_{3,22} = 407$, $P < 0.05$), with the strongest decrease (between 24% and 28%) observed in the larger species *Thalassiosira antarctica* and *Proboscia alata* (Table 3). Highest F_v/F_m was observed in *T. antarctica* ($F_{3,22} = 68.3$, $P < 0.01$) at 10 and 50 $\mu\text{mol photons} \cdot \text{m}^{-2} \cdot \text{s}^{-1}$, followed by *Pseudo-nitzschia subcurvata*, *P. alata*, and *Fragilariopsis* sp., respectively, whereas F_v/F_m was highest in *P. subcurvata* at 100 $\mu\text{mol photons} \cdot \text{m}^{-2} \cdot \text{s}^{-1}$ ($F_{3,22} = 68.3$, $P < 0.05$; Table 3). The SSE showed no clear relationship between biovolume and F_v/F_m (Table 1).

All diatom species showed high levels of NPQ upon short term high irradiance exposure (Fig. 5). In general, the contribution of NPQ_s to total NPQ was low and a large fraction of NPQ (77%–98%) was related to NPQ_F . Acclimation to the different irradiances affected NPQ in various ways. In *Fragilariopsis* sp., highest levels of total NPQ and NPQ_F were found at 50 μmol

photons $\cdot \text{m}^{-2} \cdot \text{s}^{-1}$, followed by 100 and 10 μmol photons $\cdot \text{m}^{-2} \cdot \text{s}^{-1}$, respectively ($F_{2,22} = 15.9$, $F_{2,22} = 22.1$, $P < 0.01$), whereas NPQs decreased at higher irradiances ($F_{2,22} = 8.84$, $P < 0.001$). In *Pseudo-nitzschia subcurvata*, total NPQ and NPQ_F increased, whereas NPQ_S decreased at higher irradiances ($F_{2,22} = 15.9$, $F_{2,22} = 22.1$, $F_{2,22} = 8.84$, $P < 0.05$). In *Thalassiosira antarctica*, total NPQ showed a decreasing trend with increasing irradiance (not significant), whereas NPQ_S decreased at higher irradiances ($F_{2,22} = 8.84$, $P < 0.05$) and NPQ_F remained unaffected by irradiance. And in *Proboscia alata*, highest levels of total NPQ and NPQ_F were found at 50 μmol photons $\cdot \text{m}^{-2} \cdot \text{s}^{-1}$ compared to 10 and 100 μmol photons $\cdot \text{m}^{-2} \cdot \text{s}^{-1}$ ($F_{2,22} = 15.9$, $F_{2,22} = 22.1$, $P < 0.05$) and NPQ_S increased at higher irradiance ($F_{2,22} = 8.84$, $P < 0.05$). When the different diatoms

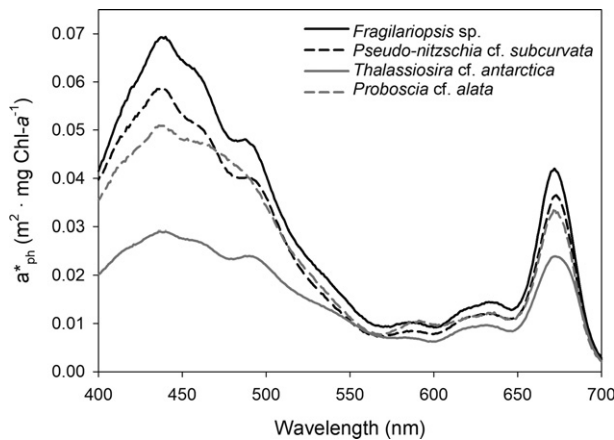


FIG. 4. Mean ($n = 3$) specific absorption coefficient $a^*_{\text{ph}}(\lambda)$ is given for *Fragilariopsis* sp. (*Fragilariopsis* sp.), *Pseudo-nitzschia* cf. *subcurvata* (Ps), *Thalassiosira* cf. *antarctica* (Ta), and *Proboscia* cf. *alata* (Pa) grown at 100 μmol photons $\cdot \text{m}^{-2} \cdot \text{s}^{-1}$.

were compared, highest levels of NPQ were found in *Fragilariopsis* sp. and *P. alata* at 50 μmol photons $\cdot \text{m}^{-2} \cdot \text{s}^{-1}$ ($F_{3,22} = 1.80$, $P < 0.05$; Fig. 5). Highest levels of NPQ_S were found in *T. antarctica*, whereas the lowest levels were found in *P. subcurvata* at 100 μmol photons $\cdot \text{m}^{-2} \cdot \text{s}^{-1}$ ($F_{3,22} = 29.0$, $P < 0.05$). Highest values of NPQ_F were found in *Fragilariopsis* sp., *P. subcurvata* and *P. alata* at 50, 100, and 50 μmol photons $\cdot \text{m}^{-2} \cdot \text{s}^{-1}$, respectively ($F_{3,22} = 5.49$, $P < 0.05$) and the four species showed similar levels of NPQ_F under all other conditions. The SSE showed a positive relationship between biovolume and NPQ and NPQ_S at lower irradiances, whereas no significant relationship with biovolume was observed for NPQ_F (Table 1).

Electron transport rates. ETR_{max} increased at higher irradiances in *Fragilariopsis* sp. ($F_{2,22} = 8.18$, $P < 0.01$) and *Thalassiosira antarctica* (not significant; Table 4). In contrast, highest ETR_{max} was found at 50 μmol photons $\cdot \text{m}^{-2} \cdot \text{s}^{-1}$ in both *Pseudo-nitzschia subcurvata* ($F_{2,22} = 8.18$, $P < 0.05$) and *Proboscia alata* (not significant). When the different diatoms were compared, ETR_{max} was highest in *T. antarctica* and *Fragilariopsis* sp. at 100 μmol photons $\cdot \text{m}^{-2} \cdot \text{s}^{-1}$ ($F_{3,22} = 3.27$, $P < 0.05$) and lowest in *Fragilariopsis* sp. at 10 μmol photons $\cdot \text{m}^{-2} \cdot \text{s}^{-1}$ ($F_{3,22} = 3.27$, $P < 0.05$). The SSE showed a relationship between biovolume and ETR_{max} at 10 μmol photons $\cdot \text{m}^{-2} \cdot \text{s}^{-1}$, but not at higher irradiances (Table 1). α_{ETR} increased at higher irradiances in the smaller species *Fragilariopsis* sp. and *P. subcurvata* ($F_{2,22} = 3.58$, $P < 0.05$), but remained unaffected by irradiance in the larger species *T. antarctica* and *P. alata* (Table 4). α_{ETR} was not significantly different between the four diatoms, but showed a decreasing trend with size at higher irradiances, as was also evident from the SSE (Tables 1 and 4). Ek_{ETR} showed an increasing trend with irradiance in *Fragilariopsis* sp. and *T. antarctica*, remained unaffected by irradiance in *P. subcurvata*

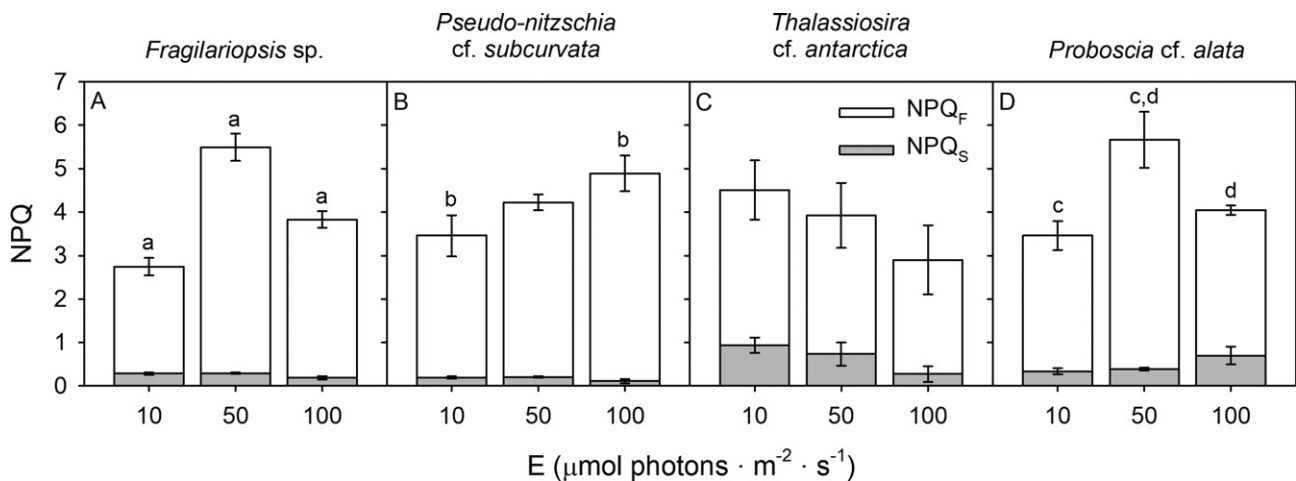


FIG. 5. Mean (\pm SD, $n = 3$) non-photochemical quenching (NPQ) is given for the four Antarctic diatom species (A) *Fragilariopsis* sp., (B) *Pseudo-nitzschia* cf. *subcurvata*, (C) *Thalassiosira* cf. *antarctica*, and (D) *Proboscia* cf. *alata* grown at 10, 50, and 100 μmol photons $\cdot \text{m}^{-2} \cdot \text{s}^{-1}$. The contribution of fast relaxing non-photochemical quenching (NPQ_F) to total NPQ is indicated by light gray and the contribution of slowly relaxing non-photochemical quenching (NPQ_S) to total NPQ is indicated by white. Significant differences ($P < 0.05$) in total NPQ between the different irradiance conditions for each diatom species are indicated by identical letters.

TABLE 4. Mean (\pm SD, $n = 3$) maximum electron transport rate (ETR_{max} in $\text{mol e}^- \cdot \mu\text{g Chl } a^{-1} \cdot \text{h}^{-1}$), initial slope of electron transport (α_{ETR} in $\text{mol e}^- \cdot \mu\text{g Chl } a^{-1} \cdot \text{h}^{-1}$), maximum electron transport (P_{max} in $\mu\text{g C} \cdot \mu\text{g Chl } a^{-1} \cdot \text{h}^{-1}$), photoacclimation index for electron transport (Ek_{ETR} in $\mu\text{mol photons} \cdot \text{m}^{-2} \cdot \text{s}^{-1}$), maximum rate of carbon fixation (P_{max} in $\mu\text{g C} \cdot \mu\text{g Chl } a^{-1} \cdot \text{h}^{-1}$), initial slope of carbon fixation (α in $\mu\text{g C} \cdot \mu\text{g Chl } a^{-1} \cdot \text{h}^{-1}$), photoacclimation index for carbon fixation (Ek in $\mu\text{mol photons} \cdot \text{m}^{-2} \cdot \text{s}^{-1}$), and photoinhibition of carbon fixation (β in $\mu\text{g C} \cdot \mu\text{g Chl } a^{-1} \cdot \text{h}^{-1}$ ($\mu\text{mol photons} \cdot \text{m}^{-2} \cdot \text{s}^{-1}$)) are given for the four Antarctic diatom species *Fragilariopsis* sp., *Pseudo-nitzschia* cf. *subcurvata*, *Thalassiosira* cf. *antarctica*, and *Proboscia* cf. *alata* grown at 10, 50, and 100 $\mu\text{mol photons} \cdot \text{m}^{-2} \cdot \text{s}^{-1}$. Significant differences ($P < 0.05$) between the different irradiance conditions for each diatom species are indicated by identical letters.

	<i>Fragilariopsis</i> sp.	<i>Pseudo-nitzschia</i> cf. <i>subcurvata</i>	<i>Thalassiosira</i> cf. <i>antarctica</i>	<i>Proboscia</i> cf. <i>alata</i>
ETR_{max}				
10 $\mu\text{mol photons} \cdot \text{m}^{-2} \cdot \text{s}^{-1}$	0.068 ± 0.025^a	$0.131 \pm 0.023^{b,c}$	0.249 ± 0.084	0.166 ± 0.003
50 $\mu\text{mol photons} \cdot \text{m}^{-2} \cdot \text{s}^{-1}$	0.173 ± 0.011^a	0.254 ± 0.033^b	0.219 ± 0.081	0.206 ± 0.059
100 $\mu\text{mol photons} \cdot \text{m}^{-2} \cdot \text{s}^{-1}$	0.307 ± 0.007^a	0.206 ± 0.003^c	0.328 ± 0.106	0.151 ± 0.011
α_{ETR}				
10	$2.15 \times 10^{-3} \pm 6.56 \times 10^{-4a}$	$2.74 \times 10^{-3} \pm 6.02 \times 10^{-4b,c}$	$3.62 \times 10^{-3} \pm 1.43 \times 10^{-3}$	$3.57 \times 10^{-3} \pm 6.25 \times 10^{-4}$
50	$4.20 \times 10^{-3} \pm 8.19 \times 10^{-4}$	$4.53 \times 10^{-3} \pm 3.56 \times 10^{-4b}$	$2.83 \times 10^{-3} \pm 9.03 \times 10^{-4}$	$2.92 \times 10^{-3} \pm 9.11 \times 10^{-4}$
100	$5.55 \times 10^{-3} \pm 1.19 \times 10^{-3a}$	$4.51 \times 10^{-3} \pm 9.36 \times 10^{-5c}$	$3.63 \times 10^{-3} \pm 3.67 \times 10^{-4}$	$3.74 \times 10^{-3} \pm 3.14 \times 10^{-4}$
Ek_{ETR}				
10	31.5 ± 1.95	48.3 ± 6.56	70.0 ± 4.72	47.8 ± 10.32
50	45.0 ± 14.60	56.0 ± 4.41	76.4 ± 3.69	74.4 ± 26.86
100	56.7 ± 10.11	45.7 ± 1.63	88.9 ± 21.14	40.5 ± 0.60
P_{max}				
10	1.39 ± 0.179^a	$2.64 \pm 0.149^{b,c}$	2.03 ± 0.164^d	1.99 ± 0.765
50	2.86 ± 1.075	3.65 ± 0.436^b	1.62 ± 0.136^c	1.80 ± 0.380
100	4.95 ± 1.174^a	3.65 ± 0.026^c	$3.47 \pm 1.316^{d,e}$	2.93 ± 0.362
α				
10	$0.179 \pm 5.12 \times 10^{-2}$	$0.062 \pm 2.77 \times 10^{-3}$	$0.054 \pm 1.65 \times 10^{-2}$	$0.063 \pm 1.05 \times 10^{-2}$
50	$0.125 \pm 4.43 \times 10^{-2}$	$0.071 \pm 6.44 \times 10^{-3}$	$0.062 \pm 2.18 \times 10^{-2}$	$0.053 \pm 1.43 \times 10^{-2}$
100	$0.079 \pm 1.69 \times 10^{-2}$	$0.075 \pm 1.14 \times 10^{-2}$	$0.062 \pm 1.30 \times 10^{-3}$	$0.051 \pm 7.32 \times 10^{-3}$
Ek				
10	8.5 ± 3.89^a	42.5 ± 4.21	41.2 ± 16.29	31.2 ± 8.72
50	22.0 ± 1.84^b	51.7 ± 8.74	28.7 ± 11.80	36.5 ± 13.26
100	$68.0 \pm 9.12^{a,b}$	49.3 ± 7.16	56.0 ± 21.62	57.0 ± 1.07
β				
10	$6.80 \times 10^{-4} \pm 2.34 \times 10^{-4a}$	$1.22 \times 10^{-3} \pm 3.18 \times 10^{-4}$	$5.50 \times 10^{-4} \pm 3.61 \times 10^{-5}$	$3.77 \times 10^{-4} \pm 2.62 \times 10^{-4c}$
50	$7.75 \times 10^{-4} \pm 2.12 \times 10^{-5b}$	$8.03 \times 10^{-4} \pm 2.90 \times 10^{-4}$	$8.27 \times 10^{-4} \pm 3.86 \times 10^{-4}$	$6.07 \times 10^{-4} \pm 2.64 \times 10^{-4d}$
100	$1.32 \times 10^{-3} \pm 4.58 \times 10^{-5a,b}$	$7.55 \times 10^{-4} \pm 1.48 \times 10^{-4}$	$9.40 \times 10^{-4} \pm 2.52 \times 10^{-4}$	$1.05 \times 10^{-3} \pm 5.66 \times 10^{-5c,d}$

and was highest at $50 \mu\text{mol photons} \cdot \text{m}^{-2} \cdot \text{s}^{-1}$ in *P. alata* (Table 4). *Thalassiosira antarctica* acclimated to higher irradiances compared to the other three diatom species ($F_{3,22} = 10.3$, $P < 0.05$), whereas Ek_{ETR} was similar between *Fragilariopsis* sp., *Pseudo-nitzschia subcurvata*, and *Proboscia alata* (except for *Fragilariopsis* sp. at $10 \mu\text{mol photons} \cdot \text{m}^{-2} \cdot \text{s}^{-1}$). The SSE showed a positive relationship between biovolume and Ek_{ETR} at $10 \mu\text{mol photons} \cdot \text{m}^{-2} \cdot \text{s}^{-1}$ (Table 1).

Carbon fixation rates. P_{max} increased at higher irradiances in all species ($F_{2,21} = 26.8$, $P < 0.05$, except for *Proboscia alata*) with the strongest increase (356%) observed in *Fragilariopsis* sp. (Table 4). Irradiance affected the comparison between the different diatoms. At the lowest irradiance, P_{max} was lowest in *Fragilariopsis* sp. and highest in *Pseudo-nitzschia subcurvata* ($F_{3,21} = 7.88$, $P < 0.05$). At $50 \mu\text{mol photons} \cdot \text{m}^{-2} \cdot \text{s}^{-1}$, P_{max} was higher in the smaller species *Fragilariopsis* sp. and *P. subcurvata* compared to the larger species *Thalassiosira antarctica* and *P. alata* ($F_{3,21} = 7.88$, $P < 0.05$). And at the highest irradiance, *Fragilariopsis* sp. showed highest P_{max} ($F_{3,21} = 7.88$, $P < 0.01$), whereas P_{max} was similar for the other three species (Table 4). Overall, *Fragilariopsis* sp. showed both lowest and highest P_{max} at 10 and $100 \mu\text{mol photons} \cdot \text{m}^{-2} \cdot \text{s}^{-1}$, respectively ($F_{3,21} = 7.88$, $P < 0.05$) and no clear trend with biovolume was observed (Table 1). α showed a decreasing trend with irradiance in *Fragilariopsis* sp., whereas α remained unaffected by irradiance in the other three Antarctic diatom species (Table 4). *Fragilariopsis* sp. showed highest α at 10 and $50 \mu\text{mol photons} \cdot \text{m}^{-2} \cdot \text{s}^{-1}$ ($F_{3,21} = 23.2$, $P < 0.01$), whereas α was similar in *P. subcurvata*, *T. antarctica* and *P. alata*. In addition, the SSE showed a negative relationship between biovolume and α (Table 1). Ek increased significantly with irradiance in *Fragilariopsis* sp. ($F_{2,21} = 18$, $P < 0.01$) and a similar trend was observed in *T. antarctica* and *P. alata* (not significant), whereas Ek was unaffected by irradiance in *P. subcurvata* (Table 4). Related to the strong increase in Ek with irradiance, *Fragilariopsis* sp. showed both lowest and highest Ek at 10 and $100 \mu\text{mol photons} \cdot \text{m}^{-2} \cdot \text{s}^{-1}$, respectively, compared to the other Antarctic diatom species ($F_{3,21} = 2.44$, $P < 0.05$). A positive relationship between biovolume and Ek was observed at $10 \mu\text{mol photons} \cdot \text{m}^{-2} \cdot \text{s}^{-1}$, but not at higher irradiances (Table 1). β increased with irradiance in *Fragilariopsis* sp., *T. antarctica* and *P. alata* ($F_{2,21} = 3.57$, $P < 0.05$, not significant for *T. antarctica*), whereas β showed a decreasing trend at higher irradiances in *P. subcurvata* (not significant; Table 4). β was similar among the four Antarctic diatom species at $50 \mu\text{mol photons} \cdot \text{m}^{-2} \cdot \text{s}^{-1}$, whereas *P. subcurvata* and *Fragilariopsis* sp. showed highest β at 10 and $100 \mu\text{mol photons} \cdot \text{m}^{-2} \cdot \text{s}^{-1}$, respectively ($F_{3,21} = 2.37$, $P < 0.05$). No clear relationship with biovolume was observed for β (Table 1).

Electron requirement of carbon fixation. In all species, $\Phi_{\text{e,C}}$ was higher than the theoretical value of $4\text{--}6 \text{ mol}$

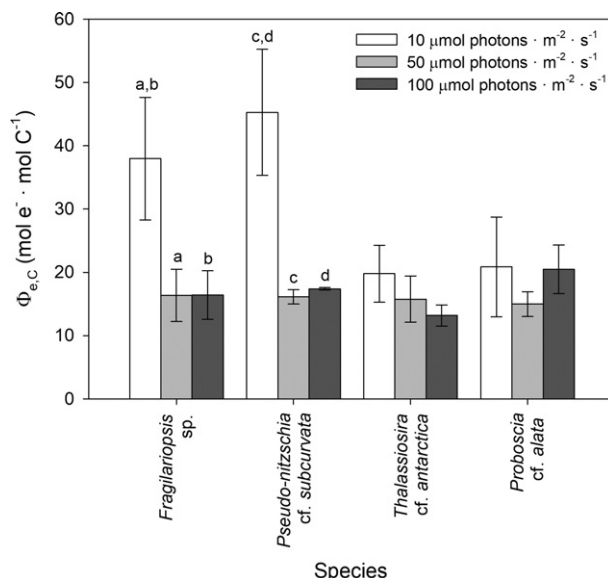


FIG. 6. Mean (\pm SD, $n = 3$) electron requirement for carbon fixation ($\Phi_{\text{e,C}}$ in $\text{mol e}^{-} \cdot \text{mol C}^{-1}$) are given for the four Antarctic diatom species *Fragilariopsis* sp. (*Fragilariopsis* sp.), *Pseudo-nitzschia* cf. *subcurvata* (Ps), *Thalassiosira* cf. *antarctica* (Ta), and *Proboscia* cf. *alata* (Pa) grown at 10, 50, and $100 \mu\text{mol photons} \cdot \text{m}^{-2} \cdot \text{s}^{-1}$. Significant differences ($P < 0.05$) between the different irradiance conditions for each diatom species are indicated by identical letters.

$\text{e}^{-} \cdot \text{mol C}^{-1}$ and ranged from 13.2 ± 1.67 to $45.3 \pm 1.14 \text{ mol e}^{-} \cdot \text{mol C}^{-1}$ (Fig. 6). $\Phi_{\text{e,C}}$ was significantly higher at 10 compared to 50 and $100 \mu\text{mol photons} \cdot \text{m}^{-2} \cdot \text{s}^{-1}$ in *Fragilariopsis* sp. and *Pseudo-nitzschia subcurvata* ($F_{2,22} = 28.2$, $P < 0.05$), whereas $\Phi_{\text{e,C}}$ was similar among the different irradiances in *Thalassiosira antarctica* and *Proboscia alata*. The smaller species *Fragilariopsis* sp. and *Pseudo-nitzschia subcurvata* showed significantly higher $\Phi_{\text{e,C}}$ compared to the larger species *T. antarctica* and *P. alata* at the lowest irradiance of $10 \mu\text{mol photons} \cdot \text{m}^{-2} \cdot \text{s}^{-1}$ ($F_{2,22} = 6.92$, $P < 0.05$), but $\Phi_{\text{e,C}}$ was similar between the different diatoms at higher irradiances. A similar trend was observed in the SSE (Table 1).

DISCUSSION

In northern Marguerite Bay, the onset of the phytoplankton bloom and the distribution of specific diatom species are related to water column stability and the consequent irradiance climate phytoplankton experience (Clarke et al. 2008, Venables et al. 2013). Despite the observation of different cell size classes throughout the phytoplankton growth season, little is known about the role of size-dependent photophysiological responses in bloom formation and succession of Antarctic diatoms. Strong size related differences in growth rate were observed in this study, with the smaller species *Fragilariopsis* sp. and *Pseudo-nitzschia subcurvata* showing much higher growth rates compared to the larger species *Thalassiosira antarctica* and *Proboscia*

alata, especially at higher irradiances. Growth rates of *Fragilariopsis* sp. and *P. subcurvata* were within the range reported for other small Antarctic diatom species (Boelen et al. 2011, Trimborn et al. 2013, Zhu et al. 2016), whereas growth rates in *T. antarctica* and *P. alata* were somewhat lower compared to earlier reports for larger Antarctic diatoms species (Timmermans et al. 2001a, Heiden et al. 2017). The negative relationship between cell size and growth has previously been reported for temperate diatoms and other phytoplankton species and has been associated with variations in light harvesting capacity and photoinhibition at high and/or excessive irradiances (Agustí 1991, Finkel 2001, Key et al. 2010).

In this study, *Fragilariopsis* sp., *Pseudo-nitzschia subcurvata*, and *Proboscia alata* showed very similar photophysiology and photoacclimation in response to increasing irradiances. These three Antarctic diatom species showed a reduction in cellular chlorophyll *a* concentrations and subsequent changes in the carbon to chlorophyll *a* ratio upon acclimation to higher irradiances, which has been observed in many other phytoplankton species from both temperate and polar regions (Falkowski and LaRoche 1991, Kropuenske et al. 2009, Arrigo et al. 2010). The decrease in cellular chlorophyll *a* in *Fragilariopsis* sp., *P. subcurvata*, and *P. alata* was associated with an increase in chlorophyll *a* specific absorption. *Thalassiosira antarctica* deviated from these trends with similar concentrations of cellular chlorophyll *a* and chlorophyll *a* specific absorption under various irradiance conditions. Despite the contrasting observations in *T. antarctica*, both cellular chlorophyll *a* and absorption per chlorophyll *a* were related to cell size and biovolume. Earlier research in Antarctic diatoms species suggested that smaller species thrive under lower irradiance conditions compared to larger species (Karentz et al. 1991, Timmermans et al. 2001a, b). This study showed that this is related to relative high pigment concentrations, high pigment absorption, and high ETR in smaller Antarctic diatoms, which has also been observed in temperate centric diatoms (Finkel 2001, Key et al. 2010). Moreover, the relationship between size and the light harvesting processes became stronger at higher irradiances, confirming earlier theoretical based observations that photoacclimation affects the size scaling of photophysiology and growth (Mei et al. 2009).

In contrast to light harvesting processes, photoprotection and photoinhibition showed no clear relationship with cell size and/or biovolume. The concentration and activity of the xanthophyll pigment cycle was uniform among the four different Antarctic diatom species, with significantly higher xanthophyll cycle pigment concentrations and activity at higher irradiances. This has previously been observed in other Antarctic diatom species such as *Chaetoceros brevis* and *Fragilariopsis cylindrus* (Kropuenske et al. 2009, Van de Poll et al. 2009, Arrigo et al. 2010, Boelen et al. 2011). In addition, high levels of NPQ were found in the studied diatom

species, which were higher compared to those previously reported for other Antarctic phytoplankton species (Alderkamp et al. 2012, Trimborn et al. 2013, Hoppe et al. 2015), but similar to the Antarctic diatom *C. brevis* and natural phytoplankton communities (Van De Poll et al. 2011). In this study, levels of NPQ_F were not directly related to the de-epoxidation of the xanthophyll pigment cycle. It has earlier been suggested that NPQ can be underestimated in Antarctic diatoms at higher irradiances due to a persistent proton gradient across the thylakoid membrane and the consequent slow epoxidation of the xanthophyll pigment cycle (Goss et al. 2006, Kropuenske et al. 2009). The high levels of photoprotection resulted in relatively low photoinhibition in the four Antarctic diatom species, as has previously been reported for the Antarctic diatom species *Fragilariopsis* sp. in comparison to *Phaeocystis antarctica* (Kropuenske et al. 2009, 2010). In contrast to earlier observations in temperate diatoms, the smaller Antarctic diatoms in this study did not show increased susceptibility to photoinhibition at high and/or excessive irradiances (Finkel 2001, Key et al. 2010). This suggests that photoinhibition played a limited role in size scaling of growth in Antarctic diatoms and that photoprotection is sufficient in both small and large Antarctic diatoms to acclimate to a variety of irradiance conditions.

Photosynthetic rates in the studied diatom species were within the range earlier reported for Antarctic diatoms and other phytoplankton species (Mills et al. 2010, Alderkamp et al. 2012, Hoppe et al. 2015), but were highly variable with cell size and biovolume and between irradiance conditions. Moreover, the observed electron transport and carbon fixation rates could not explain the success in growth of the smaller species *Fragilariopsis* sp. and *Pseudo-nitzschia subcurvata*, especially at the lowest and highest irradiance conditions. This suggests that photosynthetic processes downstream of PSII play an important role in the growth of the Antarctic diatoms. In this study, the relatively high electron requirement for carbon fixation of the small diatom species (versus the theoretical 4–6 mol e⁻ · mol C⁻¹; Genty et al. 1989, Sugget et al. 2009) indicated that energy is lost during the process of photosynthesis. Relatively high electron requirements have been reported in various phytoplankton species and natural phytoplankton communities (Sugget et al. 2009, Lawrenz et al. 2013) and have been associated with increased dissipation of excess energy as heat by the xanthophyll pigment cycle and/or alternative electron transport pathways (Olaizola et al. 1994, Prášil et al. 1996, Raven 2011). Although the observed patterns in photoprotection could explain the overall high electron requirements for carbon fixation in all studied species, there was no size scaling observed in photoprotection. Possibly, alternative electron transport pathways, such as connectivity between PSII reaction centers and/or

the Mehler reaction play a role in the size scaling of growth as species specific differences have been observed in various Antarctic diatoms (Trimborn et al. 2014, Heiden et al. 2017). Alternatively, carbon fixation can be limited by the activity of RuBisCO, especially at lower temperatures (Young et al. 2014). Antarctic diatoms and natural Antarctic phytoplankton communities generally have much higher cellular concentrations of RuBisCO, as well as a higher carboxylation and turnover rates at lower temperatures (Young et al. 2014). Despite these adaptations, the relatively low turnover rates of RuBisCO at low temperatures suggests that diatoms in the WAP region may be fixing carbon near their theoretical maximum rate (Young et al. 2014). Cell size may play an additional role, with smaller diatom species showing higher carbon fixation rates per RuBisCO, but larger diatom species investing in higher cellular concentrations of RuBisCO (Wu et al. 2014). Moreover, the activity and gene expression of RuBisCO decreases at lower irradiances in Antarctic diatoms (Falkowski and La Roche 1991, MacIntyre et al. 1996, Boelen et al. 2011), potentially explaining the overproduction of electrons relative to carbon fixation in *Fragilariopsis* sp. and *Pseudo-nitzschia subcurvata* at lower irradiances.

In this study, the smaller diatoms *Fragilariopsis* sp. and *P. subcurvata* showed highest growth rates, indicating that these species would be able to outcompete larger diatoms such as *Thalassiosira antarctica* and *Proboscia alata* in natural phytoplankton communities. In northern Marguerite Bay, the species composition of the phytoplankton community changes throughout the season, with smaller diatoms such as *Chaetoceros* and *Fragilariopsis* dominating the phytoplankton community during winter and early spring, whereas large centric diatoms such *Odontella*, *Thalassiosira*, and *Proboscia* dominate during the peak phytoplankton bloom (Clarke et al. 2008, Annett et al. 2010, A. Buma, pers. obs.). The observed size-dependent photophysiology of Antarctic diatoms supports the occurrence of small diatom species earlier in the phytoplankton growth season, with high light harvesting capacity and ETR and low photoinhibition in *Fragilariopsis* sp. and *P. subcurvata*. However, the success of larger diatom species during the phytoplankton bloom could not be explained by the variations observed in photophysiology. In addition to irradiance, nutrient availability might play an important role in the bottom-up control of smaller and larger Antarctic phytoplankton species (Raven 1998, Timmermans et al. 2001a, Finkel et al. 2010). In northern Marguerite Bay, the availability of trace metals is dependent on sea ice melt, glacial melt water input and wind induced mixing, whereas the availability of macronutrients is tightly coupled to phytoplankton growth (Bown et al. 2017). Early in the season, smaller phytoplankton species might benefit from low availability of trace metals due to a relatively high surface-area-to-volume ratio and low nutrient

requirement for growth (Raven 1998, Timmermans et al. 2001a, Finkel et al. 2010). Throughout the season, sea ice melt, glacial melt water input and wind induced mixing release more trace elements into the water column (Bown et al. 2017), thereby supporting growth of larger phytoplankton cells. As macronutrients are drawn down during the phytoplankton bloom, larger phytoplankton cells might benefit on short timescales due to a relatively greater storage capacity and potential lower metabolic costs of growth (Finkel et al. 2010, Key et al. 2010, Grover 2011). Variations in top-down control of small and large phytoplankton species may play an additional role during the phytoplankton bloom in Marguerite Bay. It has been shown that Antarctic phytoplankton communities dominated by smaller phytoplankton species experience higher grazing pressure compared to those dominated by larger phytoplankton species (Storm and Welschmeyer 1991, Garibotti et al. 2003, Smith and Lancelot 2004). Moreover, grazing is dependent on the density of phytoplankton cells in the water column (Landry 1993, Behrenfeld 2010, Garzio and Steinberg 2013). This suggests that low phytoplankton biomass earlier in the season will result in relatively low grazing pressure on both small and large diatoms, whereas during the phytoplankton bloom, grazing of small diatom species increases due to the relatively high abundance of these cells and relatively high grazing pressure, thereby increasing the competitive success of larger diatom species later in the season.

CONCLUSIONS

This study showed that the four Antarctic diatom species *Fragilariopsis* sp., *Pseudo-nitzschia subcurvata*, *Thalassiosira antarctica*, and *Proboscia alata* are able to acclimate to a variety of irradiance conditions found in coastal areas of the WAP. Although growth rates were related to size, differences in photophysiology and photosynthetic rates could not solely be explained by the two order of magnitude difference in cell size and biovolume of the four Antarctic diatom species. Size related differences in photosynthetic processes associated with light harvesting, as well as the efficiency of light harvesting at lower irradiances showed the potential success of smaller Antarctic diatom species early and late in the phytoplankton growth season. However, the response of the four Antarctic diatom species to various irradiance conditions could not explain the observed patterns in community size structure in northern Marguerite bay during the phytoplankton bloom, indicating that other factors such as nutrient availability and/or grazing pressure might play a more important role in the succession of different diatom species during the phytoplankton growth season in the WAP.

We thank Maria van Leeuwe for analysis of POC and the station and support staff at Rothera Research Station and the

- British Antarctic Survey who were involved in the summer 2013/2014 field campaign. This work was supported by the Netherlands Organization for Scientific Research (NWO) as part of the Netherlands Polar Programme, grant number 866.14.103 (GK), grant number 866.12.408 (WHP), and grant number 866.10.105 (PDR).
- Agustí, S. 1991. Allometric scaling of light absorption and scattering by phytoplankton cells. *Can. J. Fish Aquat. Sci.* 48:763–7.
- Alderkamp, A. C., Kulk, G., Buma, A. G. J., Visser, R. J. W., Van Dijken, G. L., Mills, M. M. & Arrigo, K. R. 2012. The effect of iron limitation on the photophysiology of *Phaeocystis antarctica* (Prymnesiophyceae) and *Fragilariopsis cylindrus* (Bacillariophyceae) under dynamic irradiance. *J. Phycol.* 48:45–59.
- Anadón, R. & Estrada, M. 2002. The FRUELA cruises. A carbon flux study in productive areas of the Antarctic Peninsula (December 1995–February 1996). *Deep Sea Res. Pt. II* 49:567–83.
- Annett, A. L., Carson, D. S., Crosta, X., Clarke, A. & Ganeshram, R. S. 2010. Seasonal progression of diatom assemblages in surface waters of Ryder Bay, Antarctica. *Polar Biol.* 33:13–29.
- Arrigo, K. R., Mills, M. M., Kropuenske, L. R., Van Dijken, G. L., Alderkamp, A. C. & Robinson, D. H. 2010. Photophysiology in two major southern ocean phytoplankton taxa: photosynthesis and growth of *Phaeocystis antarctica* and *Fragilariopsis cylindrus* under different irradiance levels. *Integr. Comp. Biol.* 50:950–66.
- Arrigo, K. R., Robinson, D. H., Worthen, D. L., Dunbar, R. B., DiTullio, G. R., VanWoert, M. & Lizotte, M. P. 1999. Phytoplankton community structure and the drawdown of nutrient and CO₂ in the Southern Ocean. *Science* 283:365–7.
- Behrenfeld, M. J. 2010. Abandoning Sverdrup's critical depth hypothesis on phytoplankton blooms. *Ecology* 91:977–89.
- Boelen, P., Van de Poll, W. H., Van der Strate, H. J., Neven, I. A., Beardall, J. & Buma, A. G. J. 2011. Neither elevated nor reduced CO₂ affects the photophysiological performance of the marine Antarctic diatom *Chaetoceros brevis*. *J. Exp. Mar. Bio. Ecol.* 406:38–45.
- Bown, J., Laan, P., Ossebaar, S., Bakker, K., Rozema, P. D. & De Baar, H. J. W. 2017. Bioactive trace metal time series during Austral summer in Ruder Bay, Western Antarctic Peninsula. *Deep Sea Res. Pt. II* 139:103–29.
- Clarke, A., Meredith, M. P., Wallace, M. I., Brandon, M. A. & Thomas, D. N. 2008. Seasonal and interannual variability in temperature, chlorophyll and macronutrients in northern Marguerite Bay, Antarctica. *Deep Res. Part II Top. Stud. Oceanogr.* 55:1988–2006.
- Ducklow, H. W., Baker, K., Martinson, D. G., Quetin, L. B., Ross, R. M., Smith, R. C., Stammerjohn, S. E., Vernet, M. & Fraser, W. 2007. Marine pelagic ecosystems: the West Antarctic Peninsula. *Phil. Trans. R. Soc. B.* 362:67–94.
- Falkowski, P. G. & LaRoche, J. 1991. Acclimation to spectral irradiance in algae. *J. Phycol.* 27:8–14.
- Finkel, Z. V. 2001. Light absorption and size scaling of light limited metabolism in marine diatoms. *Limnol. Oceanogr.* 46:86–94.
- Finkel, Z. V., Beardall, J., Flynn, K. J., Quigg, A., Rees, T. A. V. & Raven, J. A. 2010. Phytoplankton in a changing world: cell size and elemental stoichiometry. *J. Plankton Res.* 32:119–37.
- Garibotti, I., Vernet, M., Ferrario, M., Smith, R., Ross, R. & Quetin, L. 2003. Phytoplankton spatial distribution patterns along the western Antarctic Peninsula (Southern Ocean). *Mar. Ecol. Prog. Ser.* 261:21–39.
- Garzio, L. M. & Steinberg, D. K. 2013. Microzooplankton community composition along the Western Antarctic Peninsula. *Deep Sea Res. Pt. I* 77:36–49.
- Genty, B., Briantais, J. M. & Baker, N. R. 1989. The relationship between the quantum yield of photosynthetic electron transport and quenching of chlorophyll fluorescence. *Biochim. Biophys. Acta* 990:87–92.
- Grover, J. P. 2011. Resource storage and competition with spatial and temporal variation in resource availability. *Am. Nat.* 178: E124–48.
- Goss, R., Pintob, E. A., Wilhelma, C. & Richter, M. 2006. The importance of a highly active and DpHregulated diatoxanthin epoxidase for the regulation of the PS II antenna function in diadinoxanthin cycle containing algae. *J. Plant Physiol.* 163:1008–1021.
- Guillard, R. R. L. 1975. Culture of Phytoplankton for Feeding Marine Invertebrates. In Smith, W. L. & Chanley, M. H. (eds) *Culture of Marine Invertebrate Animals*. Springer, Boston, MA.
- Guillou, L., Bachar, D., Audic, S., Bass, D., Berney, C., Bittner, L., Boutte, C. et al. 2013. The Protist Ribosomal Reference database (PR2): a catalog of unicellular eukaryote Small Sub-Unit rRNA sequences with curated taxonomy. *Nucleic Acids Res.* 41:D597–604.
- Heiden, J. P., Bischof, K. & Trimbom, S. 2017. Light intensity modulates the response of two Antarctic diatoms species to ocean acidification. *Front. Mar. Sci.* 3:260.
- Helbling, E. W., Chalker, B. E., Dunlap, W. C., Holm-Hansen, O. & Villafañe, V. E. 1996. Photoacclimation of Antarctic marine diatoms to solar ultraviolet radiation. *J. Exp. Mar. Bio. Ecol.* 204:85–101.
- Hillebrand, H., Dürselen, C. D., Kirschtel, D., Pollinger, U. & Zohary, T. 1999. Biovolume calculation for pelagic and benthic microalgae. *J. Phycol.* 424:403–24.
- Hoppe, C. J. M., Holtz, L. & Trimbom, S. 2015. Ocean acidification decreases the light-use efficiency in an Antarctic diatom under dynamic but not constant light. *New Phytol.* 207:159–71.
- Karentz, D., Cleaver, J. & Mitchell, D. 1991. Cell survival characteristics and molecular responses of Antarctic phytoplankton to ultraviolet-B radiation. *J. Phycol.* 27:326–41.
- Key, T., McCarthy, A., Campbell, D. A., Six, C., Roy, S. & Finkel, Z. V. 2010. Cell size trade-offs govern light exploitation strategies in marine phytoplankton. *Environ. Microbiol.* 12:95–104.
- Kropuenske, L. R., Mills, M. M., Van Dijken, G. L., Alderkamp, A. C., Berg, G. M., Robinson, D. H., Welschmeyer, N. A. & Arrigo, K. R. 2010. Strategies and rates of photoacclimation in two major southern ocean phytoplankton taxa: *Phaeocystis antarctica* (Prymnesiophyceae) and *Fragilariopsis cylindrus* (Bacillariophyceae). *J. Phycol.* 46:1138–51.
- Kropuenske, L. R., Mills, M. M., Van Dijken, G. L., Bailey, S., Robinson, D. H., Welschmeyer, N. A. & Arrigo, K. R. 2009. Photophysiology in two major Southern Ocean phytoplankton taxa: photoprotection in *Phaeocystis antarctica* and *Fragilariopsis cylindrus*. *Limnol. Oceanogr.* 54:1176–96.
- Kulk, G., De Vries, P., Van De Poll, W. H., Visser, R. J. W. & Buma, A. G. J. 2012. Temperature-dependent growth and photophysiology of prokaryotic and eukaryotic oceanic picophytoplankton. *Mar. Ecol. Prog. Ser.* 466:43–55.
- Kulk, G., De Vries, P., Van De Poll, W. H., Visser, R. J. W. & Buma, A. G. J. 2013. Temperature-dependent photoregulation in oceanic picophytoplankton during excessive irradiance exposure. In Dubinsky, Z. [Ed.] *Photosynthesis*. InTech, Boulder Creek, California, pp. 209–28.
- Kulk, G., Van de Poll, W. H., Visser, R. J. W. & Buma, A. G. J. 2011. Distinct differences in photoacclimation potential between prokaryotic and eukaryotic oceanic phytoplankton. *J. Exp. Mar. Bio. Ecol.* 398:63–72.
- Landry, M. R. 1993. Estimating rates of growth and grazing mortality of phytoplankton by the dilution method. In Kemp, P. F., Sherr, B. F., Sherr, E. B. & Cole, J. J. [Eds.] *Handbook of Methods in Aquatic Microbial Ecology*. Lewis Publishers, Boca Raton, FL, pp. 715–22.
- Lawrenz, E., Silsbe, G., Capuzzo, E., Ylösto, P., Forster, R. M., Simis, S. G. H., Prášil, O. et al. 2013. Predicting the electron requirement for carbon fixation in seas and oceans. *PLoS ONE* 8:e58137.
- LeGresley, M. & McDermott, G. 2010. Counting chamber methods for quantitative phytoplankton analysis – haemocytometer, palmer-Maloney cell and Sedgewick-Rafter cell. In Bengt, K., Cusack, C. & Bresnan, E. [Eds.] *Microscopic and Molecular Methods for Quantitative Phytoplankton Analysis*. UNESCO, Paris, pp. 25–30.
- Lewis, M. & Smith, J. 1983. A small volume, short-incubation-time method for measurement of photosynthesis as a function of incident irradiance. *Mar. Ecol. Prog. Ser.* 13:99–102.

- MacIntyre, H. L., Geider, R. J. & McKay, R. M. 1996. Photosynthesis and regulation of RuBisCO activity in net phytoplankton from Delaware Bay. *J. Phycol.* 32:718–31.
- Maxwell, K. & Johnson, G. N. 2000. Chlorophyll fluorescence - a practical guide. *J. Exp. Bot.* 51:659–68.
- Mei, Z. P., Finkel, Z. V. & Irwin, A. J. 2009. Light and nutrient availability affect the size-scaling of growth in phytoplankton. *J. Theor. Biol.* 259:582–8.
- Meredith, M. P., Wallace, M. I., Stammerjohn, S. E., Renfrew, I. A., Clarke, A., Venables, H. J., Shoosmith, D. R., Souster, T. & Leng, M. J. 2010. Progress in oceanography: changes in the freshwater composition of the upper ocean west of the Antarctic Peninsula during the first decade of the 21st century. *Prog. Oceanogr.* 87:127–43.
- Mills, M. M., Kropuenske, L. R., Van Dijken, G. L., Alderkamp, A. C., Berg, G. M., Robinson, D. H., Welschmeyer, N. A. & Arrigo, K. R. 2010. Photophysiology in two southern ocean phytoplankton taxa: photosynthesis of *Phaeocystis antarctica* (Prymnesiophyceae) and *Fragilariopsis cylindrus* (Bacillariophyceae) under simulated mixed-layer irradiance. *J. Phycol.* 46:1114–27.
- Montes-Hugo, M. A., Vernet, M., Martinson, D., Smith, R. & Ianuzzi, R. 2008. Variability on phytoplankton size structure in the western Antarctic Peninsula (1997–2006). *Deep Sea Res. Pt. II* 55:2016–117.
- Olaizola, M., La Roche, J., Kolber, Z. & Falkowski, P. G. 1994. Non-photochemical fluorescence quenching and the diadinoxanthin cycle in a marine diatom. *Photosynth. Res.* 41:357–70.
- Osmond, C. B. 1994. What is photoinhibition? Some insights from comparisons of sun and shade plants. In Baker, N. R. & Bowyer, J. R. [Eds.] *Photoinhibition of Photosynthesis: From Molecular Mechanisms to the Field*. Bios Scientific Publishers, Didcot, UK, pp. 1–24.
- Perl, J. 2009. The SDSU (CHORS) method. In Hooker, S. B., Van Heukelem, L., Thomas, C. S., Claustre, H., Ras, J., Schluter, L., Clementson, L., Van der Linde, D., Eker-Develi, E., Berthon, J., Barlow, R., Sessions, H., Ismail, H. & Perl, J. [Eds.] *The Third SeaWiFS HPLC Analysis Round-Robin Experiment (SeaHARRE-3)*. NASA Tech Memo 2009–215849, NASA Goddard Space Flight Center, Greenbelt, Maryland, pp. 89–90.
- Peters, R. H. 1983. *The Ecological Implications of Body Size*, 1st Edn. Cambridge University Press, Cambridge, 344 pp.
- Piquet, A. M. T., Bolhuis, H., Meredith, M. P. & Buma, A. G. J. 2011. Shifts in coastal Antarctic marine microbial communities during and after melt water-related surface stratification. *FEMS Microbiol. Ecol.* 76:413–27.
- Platt, T., Gallegos, C. L. & Harrison, W. G. 1980. Photoinhibition of photosynthesis in natural assemblages of marine-phytoplankton. *J. Mar. Res.* 38:678–701.
- Prášil, O., Kolber, Z., Berry, J. A. & Falkowski, P. G. 1996. Cyclic electron flow around Photosystem II in vivo. *Photosynth. Res.* 48:395–410.
- Raven, J. A. 1998. The twelfth Tansley Lecture. Small is beautiful: the picophytoplankton. *Funct. Ecol.* 12:503–13.
- Raven, J. A. 2011. The cost of photoinhibition. *Physiol. Plantarum* 142:87–104.
- Rozema, P. D., Venables, H. J., Van De Poll, W. H., Clarke, A., Meredith, M. P. & Buma, A. G. J. 2017. Interannual variability in phytoplankton biomass and species composition in northern Marguerite Bay (West Antarctic Peninsula) is governed by both winter sea ice cover and summer stratification. *Limnol. Oceanogr.* 62:235–52.
- Scott, F. J. & Thomas, P. 2005. *Antarctic Marine Protists*. ABRIS & AAD, Canberra, 563 pp.
- Smith, W. O. & Lancelot, C. 2004. Bottom-up versus top-down control in phytoplankton of the Southern Ocean. *Antarct. Sci.* 16:531–9.
- Storm, S. L. & Welschmeyer, N. A. 1991. Pigment-specific rates of phytoplankton growth and microzooplankton grazing in the open subarctic Pacific Ocean. *Limnol. Oceanogr.* 36:50–63.
- Sugget, D. J., MacIntyre, H. L., Kana, T. M. & Geider, R. J. 2009. Comparing electron transport with gas exchange: parameterising exchange rates between alternative photosynthetic currencies for eukaryotic phytoplankton. *Aquat. Microb. Ecol.* 56:147–62.
- Tassan, S. & Ferrari, G. M. 1995. Proposal for the measurement of backward and total scattering by mineral particles suspended in water. *Appl. Opt.* 34:8345–53.
- Timmermans, K. R., Davey, M. S., Van der Wagt, B., Snoek, J., Geider, R. J., Veldhuis, M. J. W., Gerringa, L. J. A. & De Baar, H. J. W. 2001a. Co-limitation by iron and light of *Chaetoceros brevis*, *C. dictyota* and *C. calcitrans* (Bacillariophyceae). *Mar. Ecol. Prog. Ser.* 217:287–97.
- Timmermans, K. R., Gerringa, L. J. A., De Baar, H. J. W., Van der Wagt, B., Veldhuis, M. J. W., De Jong, J. T. M., Croot, P. L. & Boye, M. 2001b. Growth rates of large and small Southern Ocean diatoms in relation to availability of iron in natural seawater. *Limnol. Oceanogr.* 46:260–6.
- Trimborn, S., Brenneis, T., Sweet, E. & Rost, B. 2013. Sensitivity of Antarctic phytoplankton species to ocean acidification: growth, carbon acquisition, and species interaction. *Limnol. Oceanogr.* 58:997–1007.
- Trimborn, S., Thoms, S., Petrou, K., Kranz, S. A. & Rost, B. 2014. Photophysiological responses of Southern Ocean phytoplankton to changes in CO₂ concentrations: short-term versus acclimation effects. *J. Exp. Mar. Bio. Ecol.* 451:44–54.
- Van de Poll, W. H., Janknegt, P. J., Van Leeuwe, M. A., Visser, R. J. W. & Buma, A. G. J. 2009. Excessive irradiance and antioxidant responses of an Antarctic marine diatom exposed to iron limitation and to dynamic irradiance. *J. Photochem. Photobiol. B Biol.* 94:32–7.
- Van De Poll, W. H., Lagunas, M., De Vries, T., Visser, R. J. W. & Buma, A. G. J. 2011. Non-photochemical quenching of chlorophyll fluorescence and xanthophyll cycle responses after excess PAR and UVR in *Chaetoceros brevis*, *Phaeocystis antarctica* and coastal Antarctic phytoplankton. *Mar. Ecol. Prog. Ser.* 426:119–31.
- Van de Poll, W. H., Visser, R. J. W. & Buma, A. G. J. 2007. Acclimation to a dynamic irradiance regime changes excessive irradiance sensitivity of *Emiliania huxleyi* and *Thalassiosira weissflogii*. *Limnol. Oceanogr.* 52:1430–8.
- Van Heukelem, L. & Thomas, C. S. 2001. Computer-assisted high-performance liquid chromatography method development with applications to the isolation and analysis of phytoplankton pigments. *J. Chromatogr. A* 910:31–49.
- Venables, H. J., Clarke, A. & Meredith, M. P. 2013. Wintertime controls on summer stratification and productivity at the western Antarctic Peninsula. *Limnol. Oceanogr.* 58:1035–47.
- Walters, R. G. & Horton, P. 1991. Resolution of components of non-photochemical chlorophyll fluorescence quenching in barley leaves. *Photosynth. Res.* 27:121–33.
- Wu, Y., Jeans, J., Sugget, D. J., Finkel, Z. V. & Campbell, D. A. 2014. Large centric diatoms allocate more cellular nitrogen to photosynthesis to counter slower RuBisCO turnover rates. *Front. Mar. Sci.* 1:68.
- Young, J. N., Goldman, J. A. L., Kranz, S. A., Tortell, P. D. & Morel, F. M. M. 2014. Slow carboxylation of Rubisco constrains the rate of carbon fixation during Antarctic phytoplankton blooms. *New Phytol.* 205:172–81.
- Zhu, Z., Xu, K., Fu, F., Spackeen, J. L., Bronk, D. A. & Hutchins, D. A. 2016. A comparative study of iron and temperature interactive effects on diatoms and *Phaeocystis antarctica* from the Ross Sea, Antarctica. *Mar. Ecol. Prog. Ser.* 550:39–51.